SCIENCE CHINA
Information Sciences

• REVIEW •

March 2022, Vol. 65 131302:1–131302:27
https://doi.org/10.1007/s11432-021-3285-y

Key issues and algorithms of multiple-input-multiple-output over-the-air testing in the multi-probe anechoic chamber setup

Huiling PEI[1], Xiaoming CHEN[1*], Xiaoyu HUANG[1], Xiaobo LIU[1], Xiaotong ZHANG[2,3] & Yi HUANG[4]

[1]*School of Information and Communications Engineering, Xi'an Jiaotong University, Xi'an* 710049*, China;*
[2]*College of Electrical Engineering, Zhejiang University, Hangzhou* 310000*, China;*
[3]*Interdisciplinary Institute of Neuroscience and Technology, Zhejiang University, Hangzhou* 310000*, China;*
[4]*Department of Electrical Engineering and Electronics, University of Liverpool, Liverpool* L69 3GJ*, UK*

Received 1 March 2021/Revised 19 May 2021/Accepted 15 June 2021/Published online 14 February 2022

Abstract Multiple-input-multiple-output (MIMO) over-the-air (OTA) testing plays a key role in the research and development of wireless devices. MIMO OTA testing is necessary for the fifth generation (5G) wireless products, in which conventional radio frequency ports may be inaccessible. The performances of the test device can be evaluated in a repeatable and reliable way under laboratory conditions in OTA tests, which might not be feasible in conducted tests. Many efforts have been devoted to OTA test research and some achievements have been made. This paper mainly summarizes the channel emulation algorithms for two-dimensional user equipment and three-dimensional base station OTA testing in the anechoic chamber setup. In addition, the requirements of the test system design are also discussed in this paper, including the selection of the number of OTA probes, the size of the test zone, the physical dimension of the setup, and the flexible probe selection algorithm of the three-dimensional base station OTA setup. In addition, some novel test methods for 5G radio devices are also discussed.

Keywords MIMO OTA testing, multi-probe anechoic chamber, 5G, spatial channel

Citation Pei H L, Chen X M, Huang X Y, et al. Key issues and algorithms of multiple-input-multiple-output over-the-air testing in the multi-probe anechoic chamber setup. Sci China Inf Sci, 2022, 65(3): 131302, https://doi.org/10.1007/s11432-021-3285-y

1 Introduction

Multiple-input-multiple-output (MIMO) technology increases the channel capacity of the system without adding additional spectrum resources and antenna transmit power by installing multiple transmit and receive antennas at the transmitter and receiver sides, respectively. By utilizing the characteristics of the propagation channel, MIMO technology greatly improves data throughput, quality of service (QoS), and cell coverage. New wireless technologies such as long-term evolution (LTE), LTE advanced, 802.11, and the fifth generation (5G) wireless communication networks have already adopted the MIMO technology. In addition, the MIMO technology will also be widely used in the future in the sixth generation (6G) mobile communication systems [1, 2]. The massive MIMO technology is widely used in 5G millimeter wave (mmWave) communication systems. MmWave channels are very sparse because of high diffraction, penetration, and reflection losses [3]. In order to compensate for the inherent loss of high frequency and achieve high signal power, mmWave systems need to employ high-gain antennas. Fortunately, the increase of frequency means that the size of the antenna is reduced, so that the same space can accommodate more antennas, which facilitates the implementation of massive MIMO. To bring the massive MIMO technology from theory to practice, both academia and industry have invested tremendous efforts. This review focuses on both conventional MIMO and massive MIMO.

* Corresponding author (email: xiaoming.chen@mail.xjtu.edu.cn)

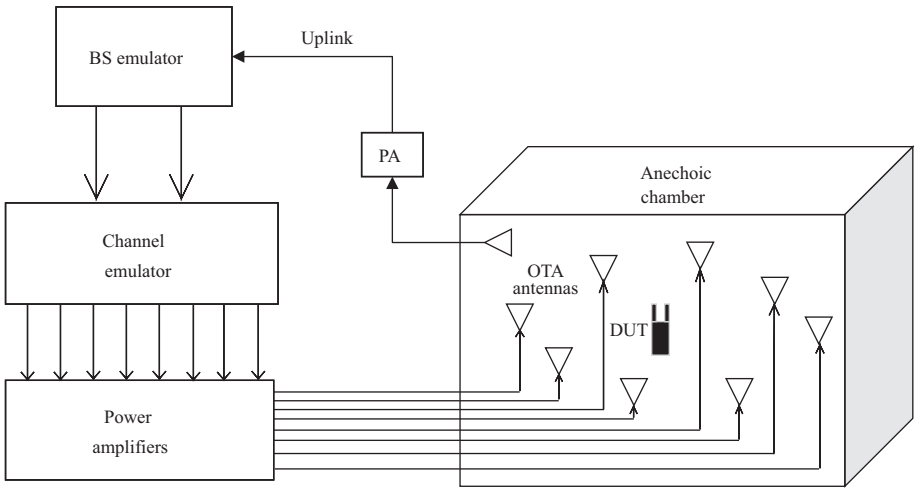

Figure 1 Illustration of the two-dimensional user equipment MIMO OTA setup.

It is important for network operators to know the radio performances of MIMO devices before massive rollout in the network. The over-the-air (OTA) testing [4,5] has been used to evaluate single-input-single-output system performance. It is also a suitable choice to assess the performances of MIMO systems. MIMO OTA testing is capable of reproducing radio propagation environment and thus can compare the different antenna configurations in the same environment [6].

Many OTA test methods have been proposed. These methods differ in how to emulate the propagation channel, system size, and cost [7–10]. There are three categories of test methods: reverberation chamber (RC) based methods [11–13], radiated two-stage (RTS) methods [14, 15], and anechoic chamber-based methods [16–18]. The RTS method evolves from the two-stage method [8] in which the "cable" connection between the channel emulator (CE) ports and the device under test (DUT) antenna ports is approached in a wireless fashion. The multi-probe anechoic chamber (MPAC) setup is capable of reproducing any realistic radio propagation channel, and all critical parts are evaluated at once [19], making it the most promising setup for MIMO OTA testing [20].

The main idea of channel emulation is to ensure correct control of the signal emitted from the probe antennas so that the emulated channel experienced by the DUT approximates the target channel. Two common channel emulation methods are pre-fading signal synthesis (PFS) [9] and plane wave synthesis (PWS). The PFS method assigns appropriate power weights to the probes to reproduce the spatial characteristics of the target channel at the receiver side [9, 21–23], whereas the PWS method assigns a suitable complex weight to each probe to reproduce the plane wave field of the target channel over the test zone. Additionally, a third method called equivalent induced voltage (EIV) [24] is also presented in this paper. It is implemented based on the similarity of the received voltages. In fact, the EIV method is also related to the field synthesis technique, because the received voltage is a response of the antenna to the electric field in the test zone.

There are many different kinds of MIMO radio channel models. Ref. [25] gave an overview of the models. The MIMO radio channel model typically includes the time, frequency, space, and polarization dimensions of the radio channel. Therefore, the model is time-varying, broadband, bidirectional, and polarized. The geometric-based random channel models are usually selected to be the target channel model, such as spatial channel model (SCM) and its extension (SCME) [26], WINNER [27], and 3GPP TR 38.901 [28]. The geometry-based modeling separates the antenna from the propagation, and the geometry and field pattern of the antenna can be defined independently of the propagation parameters.

The concept of clusters is widely used when simulating the multipath environment. A cluster has specific parameters including power angular spectrum (PAS) shape, angle of arrival (AoA), angle of departure (AoD), angle spread (AS), delay, and power. Different clusters have different delays, making the channel wideband. The PAS shape depends on the distribution of scattering components. User phantom has also been considered to achieve a more reliable performance evaluation of the MIMO device in the talk mode [29].

For standardized two-dimensional (2D) user equipment (UE) MIMO OTA testing, the DUT is in the center of the test zone, and probes are evenly distributed on a circular ring around the DUT (Figure 1).

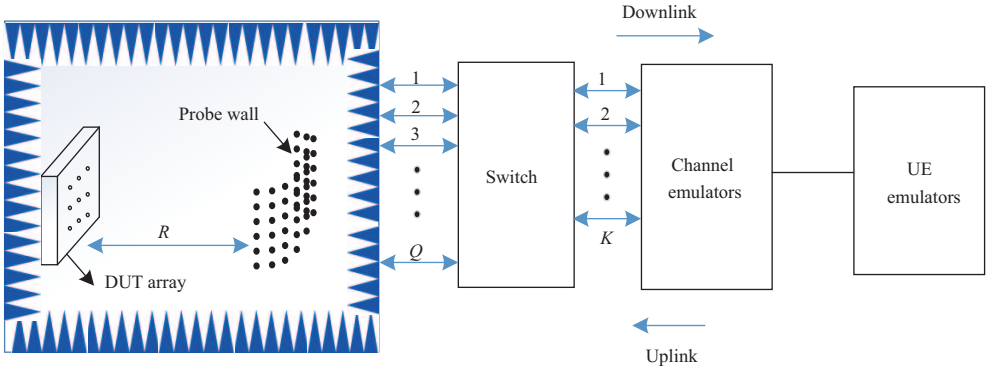

Figure 2 (Color online) Illustration of the 3D massive MIMO BS OTA setup.

The DUT is placed on a polystyrene pedestal, which supports rotation and linear motion [30]. The base station (BS) simulator is used to create the test signals. The channel simulator is used to connect to the probes to create different spatial channels [31] and can create multipath environments including path delays, Doppler spread, and fast fading. The power amplifiers adjust the signal to the desired power level [20]. The DUT is generally assumed to be in the far field of the OTA antennas.

Conventional BS antennas are tested using conducted methods, i.e., by connecting coaxial cables to the BS antenna ports. But for massive MIMO arrays, the conducted test will require hundreds of cable connections and corresponding hardware resources, which is very complicated and cost-prohibitive. A three-dimensional (3D) cost-effective test setup called 3D sectored MPAC setup is proposed for massive MIMO BS antennas OTA testing (Figure 2). This setup includes an anechoic chamber, a large number of OTA probes covering the angle area of interest, a controller used to select the active OTA antennas from the available OTA antennas, a switching circuit used to connect the active OTA antennas to the radio frequency (RF) interface ports of the CE, a DUT and a UE simulator (or multiple UEs) to mimic the UE behavior [32]. The detailed reason for choosing this test setup will be given in Section 3.

The purpose of this review is to summarize the key algorithms and issues of MIMO OTA testing in the MPAC setup. The abbreviations involved in this paper are shown in Table 1.

2 Testing of UE in 2D scenario

The channel propagation environment is 3D in the real physical world. 3D UE OTA testing has been studied in many research works, which place multiple probe rings with different elevation angles. The channel emulation technique for arbitrary 3D channel models has been described [33]. The first and last probe rings should be placed symmetrically to produce better emulation accuracy [34].

The PWS technique is more accurate than the PFS for most channel settings [35]. A specific probe setting can be found to achieve the best performance for a fixed test zone when the target channel model is determined [36]. Typically, sphere shaped test volume is usually assumed, but the ellipsoid-shaped test volume has proven to be more relevant [37]. Since we have more probes placed in the azimuth plane than in the elevation plane, the ellipsoid-shaped test zone is selected. The probe selection method has been proposed for 3D MPAC setup [38] to bring down the cost. It has revealed that the multi-shot algorithm produces the best accuracy.

However, some algorithms, e.g., [38], do not minimize the number of selected probe sets. To address this, the authors in [39] proposed the decremental selection algorithm (DSA) and the error threshold selection algorithm based on alternating search (SAAS). These algorithms minimize the number of probes while ensuring the accuracy of the target channel emulation. Notably, the SAAS provides better performance than the DSA. To further improve simulation accuracy and reduce related costs, a flexible multi-probe setup for 3D emulation has been proposed in which the probe is mounted on a movable semi-arc track for flexible probe placement at both elevation and azimuth angles. Two probe selection algorithms, i.e., the genetic and multi-shot algorithms, have been proposed to verify the feasibility and accuracy of this setup [40].

A 3D flexible MPAC setup has been proposed in [41] to achieve better compared with a fixed setup in terms of spatial correlation emulation. Another channel emulation method, called the reference method

Table 1 Abbreviation and definition

Abbreviation	Full name
2D	Two-dimensional
3D	Three-dimensional
5G	The fifth generation
6G	The sixth generation
ABC	Artificial bee colony
AoA	Angle of arrival
AoD	Angle of departure
AS	Angle spread
ASA	Azimuth spread of arrival
BS	Base station
CASA	Cluster angular spreads of arrival
CE	Channel emulator
CFR	Channel frequency response
DSA	Decremental selection algorithm
DUT	Device under test
EIV	Equivalent induced voltage
ESA	Elevation spread of arrival
EVM	Error vector magnitude
FA	Forward allocation
JADE	Joint angle and delay estimation
LOS	Line of sight
LTE	Long-term evolution
MIMO	Multiple-input-multiple-output
mmWave	Millimeter wave
MPAC	Multi-probe anechoic chamber
MU-MIMO	Multi-user MIMO
NLOS	Non-LOS
OTA	Over-the-air
PAS	Power angular spectrum
PFS	Pre-fading signal synthesis
PSO	Particle swarm optimization
PWS	Plane wave synthesis
QoS	Quality of service
RC	Reverberation chamber
RF	Radio frequency
RMS	Root mean square
RTS	Radiated two-stage
SAAS	Selection algorithm based on alternating search
SCF	Spatial correlation function
SCM	Spatial channel model
SCME	Spatial channel model extension
UE	User equipment

for 3D channel [42], managed to use a simple technique to allocate subpaths (i.e., the combination of uniform angle and power sampling). This method is more accurate than the spatial fading emulator method under the same conditions and addresses the shortcomings of the PFS method.

But, most of the standardized radio channel models such as WINNER and SCM channel models, are 2D in the sense that they use only geometrical xy-coordinates (azimuth plane). The elevation dimension has been left out due to considerably smaller angular spread in elevation than in azimuth [9]. In addition, the AS of the propagation channel is large due to the complex scattering environment at the UE side. And the 2D MIMO-OTA setup can bring down the testing system cost considerably as compared to the 3D case, which is highly desirable for relatively low cost mobile devices. Therefore, the probes in the OTA setup are distributed on the horizontal probe ring according to the 3GPP standardizations.

This section mainly summarizes channel emulation methods for 2D UE MIMO OTA testing. Metrics to

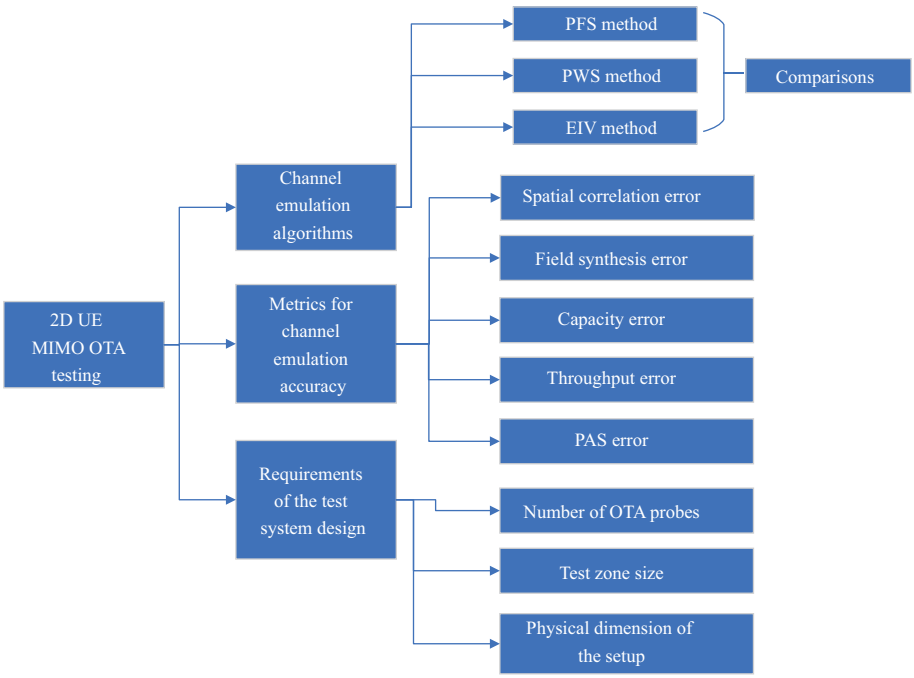

Figure 3 (Color online) Block diagram of Section 2.

evaluate the accuracy of channel emulation are also discussed. In addition, requirements for 2D MPAC setup design are also contained in this section. Typical channel emulation methods include PFS and PWS, but another technique called EIV (which focuses on reproducing target received voltage) is also described in this section. This paper does not cover the direct sampling technique because it is less accurate compared with the methods using optimized weights for the PFS technique [43–45].

Several studies, e.g., [46] have identified three factors that result in measurement inaccuracies, i.e., the pedestal instability after sledge movement, the field variation over rotation at test area center and reflections. The sources of inaccuracies are DUT placement error, cable effect, and reflections inside the chamber. For example, the cable effect will distort the radiation pattern of the DUT and hence affect the measurements [46].

Before the OTA testing, the channel model needs to be verified at the DUT location [47] to ensure that the DUT can be tested in the desired channel environment. The verification process involves some important parameters, including power delay distribution, temporal correlation, spatial correlation, and cross-polarization power ratio. The specific verification process has been described in [48].

It is important to calibrate the OTA system before conducting measurements. The main purpose of the calibration is to eliminate the non-idealities of the system such as the impact of probe placement errors on the measurement [49]. Performance deterioration caused by system non-idealities is investigated in terms of spatial characteristics in [49], whereas Ref. [50] investigated performance deterioration introduced by system non-idealities in terms of field synthesis.

Figure 3 draws a block diagram of this section for better illustration.

2.1 Channel emulation algorithms and their comparisons

2.1.1 *PFS method*

Since the PFS technique can emulate all dimensions of the standardized channel model, and only need to perform power calibration on OTA probes, it has been widely used in the industry. By convolving the transmitted signal from the BS simulator with the emulated channel impulse response from the CE, a pre-fading signal is created in the CE. The frequency and time characteristics of the fading channel are controlled by the CE. So the idea of the PFS method is to transmit power-weighted Rayleigh or any other fading signals from multiple independent probes to reproduce the spatial characteristics of the target channel measured at the receiver side. The fading signals associated with the same cluster are independent and identically distributed. Geometry-based random channel models are selected as target

channel models for the PFS technique. For a channel model with multiple clusters, an independent channel emulation is performed for each cluster. Each cluster maps to multiple probes, according to the PAS of the cluster and directions of OTA probes. Polarization is omitted in the following described PFS method, which can be readily extended to dual-polarized channel models. Spatial correlation has been selected as the metric to characterize the spatial characteristics at the Rx side. The spatial correlation is a statistical measure of the similarity of the received signals at different locations in space. The spatial correlation function (SCF) and PAS are a Fourier transform pair and the spatial correlation depends on the PAS of the channel. To reconstruct the PAS of the target channel, suitable probe power weights are generated for each cluster. The antenna correlation in the target channel can be written as

$$\rho = \frac{\int_{-\pi}^{\pi} G_{q1}(\phi) G_{q2}^{*}(\phi) P(\phi) \mathrm{d}\phi}{\sqrt{\int_{-\pi}^{\pi} P(\phi)|G_{q1}(\phi)|^2 \mathrm{d}\phi}\sqrt{\int_{-\pi}^{\pi} P(\phi)|G_{q2}(\phi)|^2 \mathrm{d}\phi}}, \tag{1}$$

where $G_{q1}(\phi)$ and $G_{q2}(\phi)$ are complex radiation patterns of antenna pair (q_1, q_2); ϕ represents the AoA of the incoming wave; $P(\phi)$ represents the continuous PAS of the target channel.

For simplicity, it is assumed that the DUT is omnidirectional. The spatial correlation of the target channel can be written as

$$\rho\left(q_1, q_2\right) = \int_{-\pi}^{\pi} \exp\left(\mathrm{j}2\pi/\lambda\left(\boldsymbol{p}_{q1} - \boldsymbol{p}_{q2}\right) \cdot \phi\right) P(\phi) \mathrm{d}\phi, \tag{2}$$

where λ is wavelength; $\boldsymbol{p}_{q1}$ and $\boldsymbol{p}_{q2}$ are position vectors of the antenna pair (q_1, q_2).

Assuming that the wave received by the DUT in the test area is an ideal plane wave, the spatial correlation of the emulated channel can be written as

$$\hat{\rho}_{\mathrm{ideal}} = \sum_{k=1}^{K} g_k \exp\left(\mathrm{j}2\pi/\lambda\left(\boldsymbol{p}_{q1} - \boldsymbol{p}_{q2}\right) \cdot \bar{\phi}_k\right), \tag{3}$$

where g_k represents the power weight of the kth probe; K is the number of the probes; $\bar{\phi}_k$ is the unit position vector of the kth probe.

Let $\boldsymbol{\rho}$ and $\hat{\boldsymbol{\rho}}_{\mathrm{ideal}}$ represent the spatial correlation vectors of the target channel and the emulated channel under the ideal plane wave assumption, respectively. The objective function is based on the above two sets of spatial correlation.

$$\min \|\hat{\boldsymbol{\rho}}_{\mathrm{ideal}}\left(\boldsymbol{g}\right) - \boldsymbol{\rho}\|_2^2. \tag{4}$$

The spatial correlation is selected as the objective function without constraints on the PAS shape [9, 22, 23, 51]. However, owing to the limited number of the test samples, different shapes of the PASs may result in similar spatial correlation. Therefore, a limitation on the shape (average AoA and AS) of the PAS is introduced; that is, the PAS of the target channel is accurately simulated by limiting the deviation between the simulated average AoA and AS and the target average AoA and AS [52]. The above quadratic programming problem with linear constraints can be easily solved by convex optimization [53]. Note that if a small anechoic chamber is used for reduced cost, the emulated spatial correlation will introduce the spherical wave effect, and the emulated spatial correlation can be written as

$$\hat{\rho}_{\mathrm{small}} = \frac{\sum_{k=1}^{K} g_k \cdot F_{k,u} F_{k,v} \exp\left(\mathrm{j}2\pi\left(d_{k,u} - d_{k,v}\right)/\lambda\right)}{\sqrt{\sum_{k=1}^{K} F_{k,u}^2 g_k \sum_{k=1}^{K} F_{k,v}^2 g_k}}, \tag{5}$$

where $F_{k,u}$ and $F_{k,v}$ are path loss terms from the kth probe to the uth and vth DUT elements, respectively; $d_{k,u}$ and $d_{k,v}$ are distances from the kth probe to the uth and vth DUT elements, respectively. In this case, the field within the test area includes both the desired signals from the probes and the undesired signals caused by reflections and coupling among the probes. Therefore, the chamber compensation technique can be used to reduce the undesired paths [54, 55].

If the DUT antenna pattern is considered, the emulated antenna correlation in the OTA case can be written as

$$\hat{\rho} = \frac{\sum_{k=1}^{K} G_{q1}\left(\phi_k\right) G_{q2}\left(\phi_k\right) g_k}{\sqrt{\sum_{k=1}^{K} |G_{q1}\left(\phi_k\right)|^2}\sqrt{\sum_{k=1}^{K} |G_{q2}\left(\phi_k\right)|^2}}. \tag{6}$$

The number of probe antennas that can achieve sufficient correlation accuracy for ideal DUTs may not achieve sufficient accuracy for realistic DUTs when the antenna pattern varies fast [24]. Therefore, DUT patterns should be considered to determine the number of probes. But for realistic DUT at sub 6 GHz, the DUT antenna pattern is quasi-omnidirectional.

Once the power weights of the probes are determined, the channel coefficients simulated by the PFS method are also determined. Note that the channel coefficients ignore the patterns of the probe antennas and the path loss of free space. There are U receiving antennas and S transmitting antennas, and for simplicity, only vertical polarization is considered.

$$\begin{aligned}\hat{h}_{u,s,n}^{\mathrm{PFS}}(t,f) =& \sqrt{\frac{P_n}{M}} \sum_{k=1}^{K} \sum_{m=1}^{M} F_s^{\mathrm{Tx}}\left(\varphi_{n,m}\right) F_u^{\mathrm{Rx}}\left(\phi_k^{\mathrm{OTA}}\right) \\ & \cdot \sqrt{g_{n,k}} \cdot \exp\left(\mathrm{j}2\pi v_{n,m} t + \mathrm{j}\Phi_{n,m,k}\right) \cdot \exp\left(-\mathrm{j}2\pi f \tau_n\right), \end{aligned} \tag{7}$$

where P_n is the power of the nth cluster; M is the number of subpaths in each cluster; F_s^{Tx} and F_u^{Rx} are the field pattern of sth Tx antenna and uth Rx antenna, respectively. Note that the field pattern is defined with a common phase center. $v_{n,m}$ is the Doppler frequency of the mth subpath of the nth cluster; τ_n is delay of the nth cluster; $\Phi_{n,m,k}$ is the random initial phase generated for each subpath of each cluster. Note that for each probe, the random initial phase is independently generated.

2.1.2 *PWS method*

The PFS technique can only reproduce channels with specific PAS shapes, while the PWS technique can reproduce dynamic multipath environments with time-varying PASs. The target field is approximated by superposing the fields from probes for the PWS method. The target field can be determined by arbitrary reference channel models, such as geometry based random channel models. Note that the probe weights are generated for each subpath instead of for each cluster. The generation of plane waves relies on assigning appropriate complex weights to different probes. The main disadvantage of the PWS method is that the probes require phase and power calibration due to complex probe weights. The PWS technique can be implemented based on plane waves [9, 56] or by using the spherical wave theory to synthesize desired electromagnetic field environment [16, 57]. Although the PWS method is traditionally based on plane waves, the spherical wave theory is preferred because it includes near-field effects during the synthesis of electromagnetic environments [18]. Therefore, the technique using the spherical wave theory supports the DUT evaluation well in the real-world operation. Another reason for the superiority of the technique based on the spherical wave theory is the well-known cut-off property of the spherical wave function, which provides a theoretical estimate of the number of probes.

For a single plane wave, according to the least squares technique [58], the optimization problem can be solved with the following equation:

$$\boldsymbol{F}\boldsymbol{W} = \boldsymbol{T}, \tag{8}$$

where $\boldsymbol{T}$ is the target field; $\boldsymbol{F}$ is the coefficient transfer matrix from the probes to the sampling points over the test area; $\boldsymbol{W}$ is the weight vector to be solved. Assuming that the M-point sampling is performed in the test area and M is greater than K (i.e., the number of probes), then the optimization problem becomes an over-determined problem, and the weight vector can be obtained by solving the following problem of minimizing the 2-norm:

$$\min_{\boldsymbol{w}} \|\boldsymbol{F}\boldsymbol{W} - \boldsymbol{T}\|. \tag{9}$$

From this, we can get

$$\boldsymbol{W} = \left(\boldsymbol{F}^{\mathrm{H}}\boldsymbol{F}\right)^{-1}\boldsymbol{T}^{\mathrm{H}}\boldsymbol{T}. \tag{10}$$

For vertical polarization, both the target field and the emulated field are perpendicular to the xy plane. For horizontal polarization, the target field is on the xy plane and perpendicular to the AoA, whereas the emulated field is on the xy plane and perpendicular to the AoA where the probe is located. To accurately emulate the horizontal polarization field, the optimization must be decomposed to two orthogonal axes x and y as

$$\min_{\boldsymbol{w}} \left\| \begin{bmatrix} \boldsymbol{F}_x \\ \boldsymbol{F}_y \end{bmatrix} \boldsymbol{W} - \begin{bmatrix} \boldsymbol{T}_x \\ \boldsymbol{T}_y \end{bmatrix} \right\|_2^2, \tag{11}$$

and it can be easily solved by convex optimization. The correlation accuracy for the two polarizations is the same for the large OTA ring radius [24].

Using spherical wave extension, the electric field of a time-harmonic plane wave from the free space can be expressed as

$$\boldsymbol{E}(r,\theta,\phi)=\frac{k}{\sqrt{\eta}}\sum_{s=1}^{2}\sum_{n=1}^{\infty}\sum_{m=-n}^{n}Q_{\mathrm{smn}}^{(1)}\boldsymbol{F}_{\mathrm{smn}}^{(1)}(r,\theta,\phi), \tag{12}$$

where k is the wave number; η is the admittance of the medium; s,m,n represent the mode index of the spherical wave; $Q_{\mathrm{smn}}^{(1)}$ is a spherical wave coefficient for a spherical standing wave; $\boldsymbol{F}_{\mathrm{smn}}^{(1)}$ is the corresponding spherical vector wave function in the standard spherical coordinates. Due to the cut-off property of the spherical wave function [59], especially that of the spherical Bessel function and its derivative function, Eq. (12) can be written as

$$\boldsymbol{E}(r,\theta,\phi)=\frac{k}{\sqrt{\eta}}\sum_{s=1}^{2}\sum_{n=1}^{N}\sum_{m=-n}^{n}Q_{\mathrm{smn}}^{(1)}\boldsymbol{F}_{\mathrm{smn}}^{(1)}(r,\theta,\phi), \tag{13}$$

where N is the truncation number, $N=\lceil kr_0+n_1\rceil$; r_0 is the radius of the test area; n_1 is a small integer used to control the accuracy of the emulation; $\lceil\cdot\rceil$ denotes round up operation. Similarly, the radiated field of a probe can be written as

$$\boldsymbol{E}_k(r,\theta,\phi)=\frac{k}{\sqrt{\eta}}\sum_{j=1}^{J}w_kP_j^kF_j^{(1)}(r,\theta,\phi), \tag{14}$$

where w_k is the voltage of the kth probe; J is the number of spherical wave modes; P_j^k is a spherical wave coefficient of the probe radiation pattern. To reproduce the target field in (13), we can obtain an equation

$$\begin{bmatrix}P_1^1 & P_1^2 & \cdots & P_1^K\\ P_2^1 & P_2^2 & \cdots & P_2^K\\ \vdots & \vdots & \ddots & \vdots\\ P_J^1 & P_J^2 & \cdots & P_J^K\end{bmatrix}\begin{bmatrix}w_1\\ w_2\\ \vdots\\ w_k\end{bmatrix}=\begin{bmatrix}Q_1\\ Q_2\\ \vdots\\ Q_J\end{bmatrix}. \tag{15}$$

This equation can be written in a matrix form like $\boldsymbol{PW}=\boldsymbol{Q}$. Then the probe voltage vector can be obtained by the Moore-Penrose pseudo-inverse as

$$\boldsymbol{W}=\boldsymbol{P}^{+}\boldsymbol{Q}=\left(\boldsymbol{P}^{\mathrm{H}}\boldsymbol{P}\right)^{-1}\boldsymbol{P}^{\mathrm{H}}\boldsymbol{Q}. \tag{16}$$

Two schemes are proposed to reproduce the time-varying SCM. In the first scheme, each snapshot of the time-varying channel is considered static and can be modeled by multiple static plane waves, each of which has a complex amplitude, AoA, and polarization. The PWS technique is applied to each snapshot to form the time-varying channel. In the second scheme, the cluster with a static PAS can be discretized by a set of plane waves with specific AoAs. The Doppler frequency shift is introduced into each static plane wave to generate the time-varying channel. If the Doppler shift is introduced to the system, the time-varying weight is obtained by multiplying the complex weight by the rotation phasor.

$$w_k(t)=w_k\exp\left(-\mathrm{j}tw_d\right)=w_k\exp\left(\mathrm{j}t\boldsymbol{\beta}\cdot\boldsymbol{v}\right), \tag{17}$$

where w_d is the Doppler shift, which can be determined by the wave vector $\boldsymbol{\beta}$ and the moving speed $\boldsymbol{v}$ of the DUT.

Once the complex weights of the probes are determined, the channel coefficients emulated by the PWS method are also determined. Note that the channel coefficients also ignore the patterns of the probe antennas and the path loss of free space.

$$\begin{aligned}\hat{h}_{u,s,n}^{\mathrm{PWS}}(t,f)=&\sqrt{\frac{P_n}{M}}\sum_{m=1}^{M}\sum_{k=1}^{K}F_s^{\mathrm{Tx}}\left(\varphi_{n,m}\right)F_u^{\mathrm{Rx}}\left(\phi_k^{\mathrm{OTA}}\right)\\ &\cdot w_{n,m,k}\cdot\exp\left(\mathrm{j}2\pi v_{n,m}t+\mathrm{j}\Phi_{n,m}\right)\cdot\exp\left(-\mathrm{j}2\pi f\tau_n\right),\end{aligned} \tag{18}$$

where $w_{n,m,k}$ is the complex weight of the kth probe of the mth subpath of the nth cluster.

If the modeling of the Ricean channel is involved, the line of sight (LOS) path can be emulated by the PWS method, whereas the other non-LOS clusters are simulated by the PFS method [60]. In this case, it should be noted that for the LOS path, power and phase calibration are both required, but only power calibration is required for other paths.

The space-time correlation analysis has been performed for the above two emulation methods [60], which revealed that the power AoA-AoD spectrum has a Kronecker structure in the PFS method.

2.1.3 *EIV technique*

The goals of the PFS and PWS methods are to reproduce the correlation at the Rx side and to reconstruct the target field within the test area, respectively. Although the PWS technique can synthesize plane waves with arbitrary AoAs, the difference between the target received voltage and induced received voltage in the OTA case is still a problem. The EIV method aims to reproduce the target received voltage by assigning appropriate complex weight to each probe. The accuracy of the received voltage depends on the field synthesis accuracy and radiated pattern of the DUT antenna.

The received voltage is not only determined by the impinging plane waves but by antenna patterns. The target received voltage can be defined as

$$V = E_0 \cdot L(\phi), \tag{19}$$

where E_0 is the electric density of the incident field and L is the antenna radiation pattern. The antenna pattern refers to the relative field strength of the radiation field in the far field area. When E_0 is constant, the induced voltage changes with the antenna pattern $L(\phi)$, which is a function of ϕ. Assume that the OTA probes radiate ideal plane waves. The emulated received voltage in the OTA case can be defined as

$$\hat{V} = \sum_{k=1}^{K} V_k = E_0 \cdot \sum_{k=1}^{K} g_k(\phi) L(\phi_k) = E_0 \cdot \hat{L}(\phi), \tag{20}$$

where $\hat{L}(\phi)$ is the emulated antenna radiation pattern in the plane wave arrival direction ϕ. Our goal is to optimize g_k to ensure that V is equal to $\hat{V}$. $g_k(\phi)$ can be obtained by using trigonometric interpolation [61] as follows:

$$g_k(\phi) = \frac{1}{K} \sum_{k=1}^{K} \cos m\left(\phi - \phi_k\right), \tag{21}$$

where $m = k - \lceil K/2 \rceil$. Then we can solve for the complex weight assuming that the phase at the test zone center is 0 as

$$g_k^{\mathrm{TI}}(\phi) = g_k(\phi) \exp\left(-\mathrm{j}\beta R\right), \tag{22}$$

where β is the wave number; R is the radius of the OTA probe ring. The EIV method generates the same complex weights as the PWS method when R is large [24].

2.1.4 *Comparisons of channel emulation algorithms*

This subsection mainly provides comparisons of channel emulation algorithms listed in Subsections 2.1.1–2.1.3.

(1) Comparison between PFS and PWS methods. Generally, the PFS and PWS techniques are considered to have almost the same emulation accuracy. However, this conclusion is only valid under certain conditions. In order to compare the emulation accuracy of the PFS and PWS methods, we conduct a series of simulations. Assume that 16 probes are evenly distributed on a circle with a radius of 2 m, that is, the angular spacing between two adjacent probes is 22.5° (Figure 4). Assume that the target channel has only a single cluster and the PAS of the cluster follows the Laplacian distribution. Two types of clusters are considered in the emulation, one of which has a mean AoA of 0° (best case) and the other has a mean AoA of 11.25° (worst case). The cluster angular spreads of arrival (CASA) changes from 5° to 30° with an interval of 5° in the emulation. By comparing the emulated SCFs of the PFS and PWS methods to the target channel for the two cases, the performances of the PFS and PWS methods are demonstrated.

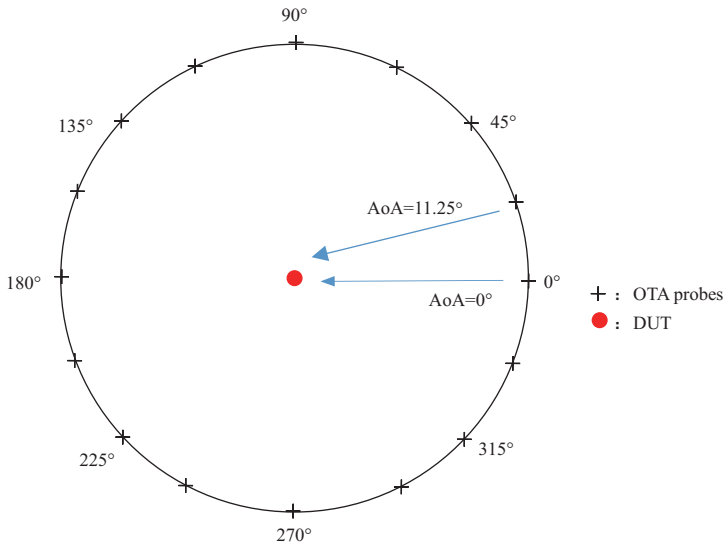

Figure 4 (Color online) The 2D OTA probe configuration for the emulation.

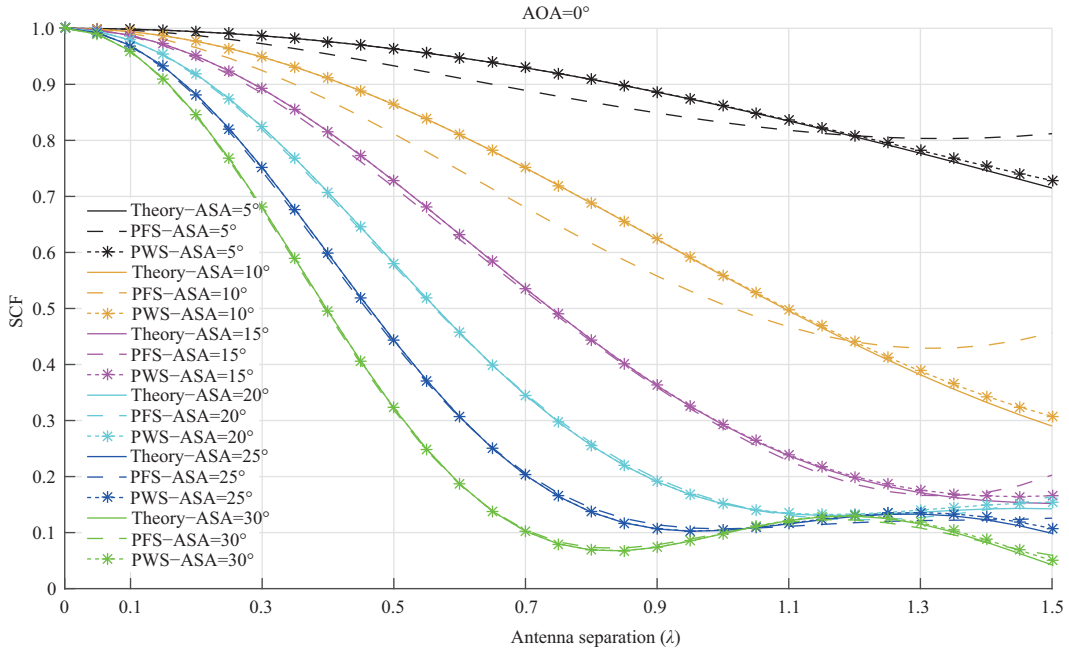

Figure 5 (Color online) Correlation for the best case.

Figures 5 and 6 show the correlation curves as a function of DUT antenna separation for the best case and worst case, respectively. It can be seen that the SCF of the PWS method follows that of the target channel well until the antenna separation grows larger than 1.5λ. This is because the PWS technique can reproduce plane waves with arbitrary AoAs in the test zone with a sufficient number of OTA probes, as demonstrated in [60]. As can be seen, the PWS method outperforms by the PFS method for both cases. The emulation deviation of both methods gradually decreases as the CASA increases. Nevertheless, it is also demonstrated that the PFS method has poor emulation performance for clusters with small CASAs. When the CASA is much smaller than the angular separation of adjacent OTA probes, the cluster becomes very specular in the angular domain, and the emulation deviation of the PFS technique in the worst case becomes more obvious. Because the cluster illuminates in the direction where no OTA probe is located, the PFS technique cannot accurately reproduce it. However, the PFS and PWS methods have almost the same emulation accuracy when the CASA is large.

(2) Comparison between PWS and EIV methods. The comparison between PWS and EIV methods is

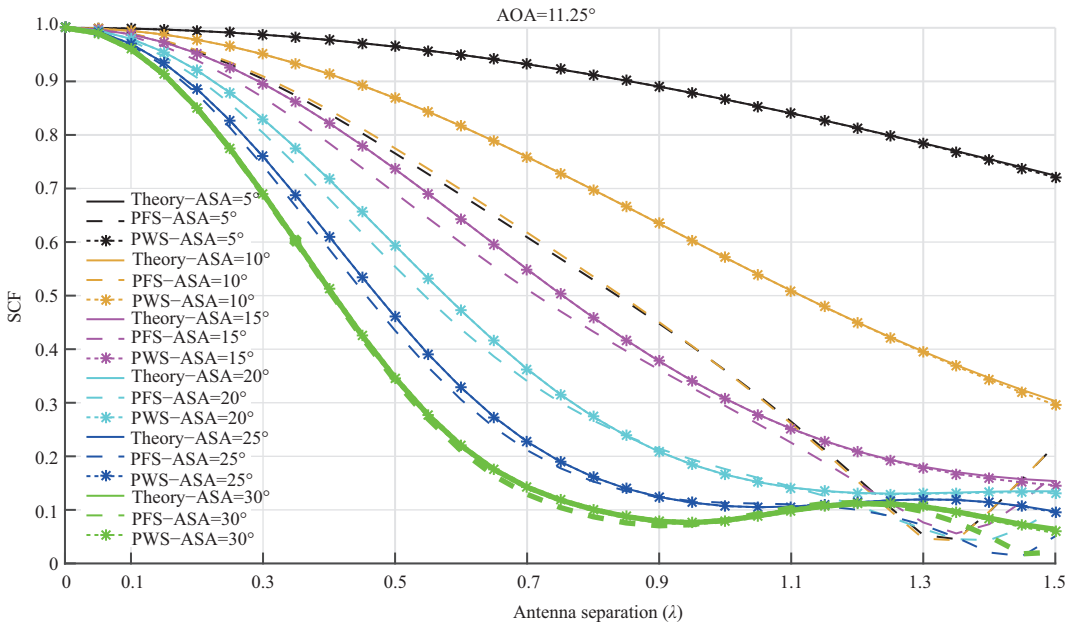

Figure 6 (Color online) Correlation for the worst case.

Table 2 Performance of three methods for 2D UE OTA testing

Channel emulation algorithm	Performance
PFS	Cost function is the deviation of spatial correlations. Not suitable for small CASA. Only power calibration is needed.
PWS	Cost function is the deviation of fields. Can accurately synthesize arbitrary plane waves. Both power and phase calibration are needed.
EIV	Cost function is the deviation of received voltages. Not suitable for small OTA probe rings. Both power and phase calibration are needed.

detailed in [24]. First, the complex weights obtained by the EIV technique are polarization independent, which is the same as the PWS technique. Second, the complex weighting matrix obtained by the PWS and EIV techniques is practically the same when the radius of the OTA ring is large. But the PWS technique has better emulation accuracy if the OTA ring radius is small. This is because accurate field synthesis does not mean accurate received voltage, and the difference is mainly due to the limited OTA ring radius.

Three channel emulation methods, namely PFS, PWS, and EIV methods, for 2D UE OTA testing are introduced and analyzed above. Table 2 summarizes the performance of the three methods.

2.2 Channel emulation accuracy

There are some metrics to evaluate how well the emulated channel approximates the target channel, including spatial correlation error, field synthesis error, capacity error, and throughput error.

(1) Spatial correlation error. The spatial correlation error, i.e., $|\rho-\hat{\rho}|$, is generally selected to evaluate the emulation accuracy for the PFS technique, where ρ and $\hat{\rho}$ represent the target and emulated spatial correlations, respectively. For example, $|\rho-\hat{\rho}|<0.1$ is used in [9]. When $|\rho|$ is high, the spatial correlation error is more critical, which means the performance of the MIMO system is sensitive to spatial correlation. On the contrary, the spatial correlation error is less critical when $|\rho|$ is small [62]. However, different shapes of PASs may result in similar spatial correlations. Therefore, in order to ensure that the spatial correlation error is a good measure of the emulation accuracy, the error threshold of the PAS needs to be added as the optimization constraint, as described in Subsection 2.1.

(2) Field synthesis error. The field synthesis error, i.e., $|E-\hat{E}|$, is generally selected to evaluate the emulation accuracy for the PWS technique, where E and $\hat{E}$ represent the target and emulated field, respectively [58]. -15 dB is usually used as the error threshold of the error vector magnitude (EVM) of

the electric field. EVM is defined as

$$\mathrm{EVM} = 10\log_{10}\frac{\|E-\hat{E}\|_2^2}{\|E\|_2^2}. \tag{23}$$

(3) Capacity error. However, the spatial correlation error and the field synthesis error cannot directly reflect the data rate error. Thus, the channel capacity error is proposed in [63]. MIMO channel matrix in the frequency domain has been obtained in Subsections 2.1 and 2.2. We assume that the channel state information is not available on the Tx side. Therefore, equal power is assumed among Tx antennas, and the channel capacity is calculated based on this assumption. The instantaneous channel capacity of the target channel can be written as [64]

$$C(t) = \frac{\sum_{n_f=1}^{N_f}\log_2\det(\boldsymbol{I}+\frac{\sigma}{\eta\cdot S}\cdot\boldsymbol{H}(t,n_f)\cdot\boldsymbol{H}(t,n_f)^{\mathrm{H}})}{N_f}, \tag{24}$$

where N_f is the number of subcarriers; σ is signal to noise ratio; S is the number of Tx antennas; η is the power normalization factor to ensure the received power is one. Note that N_f has to be large enough to ensure that each sub-channel experiences flat fading.

Let C and $\hat{C}$ represent the target and emulated channel capacities, respectively. Then the capacity error is defined as $|C-\hat{C}|$. The channel capacity error threshold is set to 0.2 bits/s/Hz in [63]. When the correlation at the transmit side is high, both the target and emulated channel capacities are low, and the correlation at the receive side is irrelevant to the simulation accuracy. Therefore, the size of the test area is usually limited when the spatial correlation at the transmit side is low. Furthermore, when the target spatial correlation at the receive side is small, the channel capacity accuracy is less sensitive to the spatial correlation accuracy.

(4) Throughput error. The channel capacity only indicates the theoretical upper bound of the data rate, and cannot directly reflect practical MIMO terminal performance [62]. Throughput error is used to characterize the channel emulation accuracy in order to reflect the end-to-end performance of the system. Throughput error is defined as the difference between the target and emulated throughputs. The measurement method of the system throughput will be described in Subsection 2.3.2. The throughput error needs to be measured when the correlation at the BS side is small to obtain real measurement performance, which is the same as channel capacity error. Moreover, when the target spatial correlation at the receive side is small, the throughput accuracy is also less sensitive to the spatial correlation accuracy.

In summary, the spatial correlation error is usually used to characterize the OTA simulation accuracy for the PFS technique, but it is necessary to pay attention to adopt the PAS error in the constraints of the PFS optimization. The field synthesis error is selected to express the simulation accuracy for the PWS technique. It is more appropriate to use the channel capacity error or the throughput error as the metric to measure the emulation accuracy, and the throughput error is more concerned with the real end-to-end performance of the system.

2.3 Rrequirements of the 2D UE test system design

2.3.1 *Number of OTA probes*

The number of required OTA antennas in the MPAC setup has been studied in many literatures. Studies have shown that the number of OTA probes is related to the DUT size, channel model, OTA probe locations, and acceptable error levels for the metrics discussed in Subsection 2.2. A rule of thumb of the number of OTA antennas is shown in [9]. General rules for the required number of probes have been proposed [65–69]. In theory, an infinite number of OTA antennas are required to synthesize any electromagnetic field over the test zone, which is unrealistic. From (13), we can solve for the number of spherical wave modes using $J = 2N(N+2) = 2(\lceil kr_0+n_1\rceil)^2 + 4(\lceil kr_0+n_1\rceil)$. To accurately generate these J modes, the minimum number of probes should be equal to J, i.e.,

$$K_{\mathrm{MIN}} = 2\left(\lceil kr_0+n_1\rceil\right)^2 + 4\left(\lceil kr_0+n_1\rceil\right). \tag{25}$$

Eq. (25) considers the 3D case, but because the elevation angle range near the UE is typically narrow, the elevation angle is often assumed to be fixed at 90°. Then the 3D case is simplified to the 2D case,

Table 3 n_1 for different equivalent reflectivity levels

Equivalent reflectivity level ε	n_1
−10 dB	$0.37 \times \sqrt[3]{kr_0}$
−15 dB	$0.74 \times \sqrt[3]{kr_0}$
−20 dB	$1.08 \times \sqrt[3]{kr_0}$
−25 dB	$1.45 \times \sqrt[3]{kr_0}$
−30 dB	$1.85 \times \sqrt[3]{kr_0}$

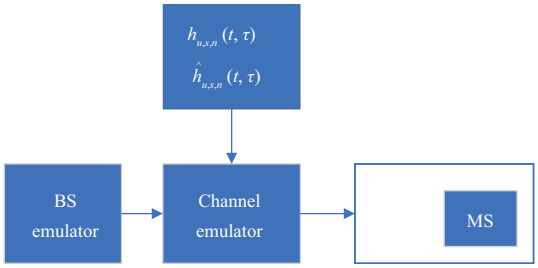

Figure 7 (Color online) Synthetic MPAC setup.

with the mode number J changed to $J = K_{\mathrm{MIN}}^{2D} = 2(2N+1) = 4(\lceil kr_0 + n1 \rceil) + 2$. To obtain a more accurate number of probes in the 2D case, the value of n_1 is crucial. The relation between n_1 and test zone size r_0 is $n_1 = o(\sqrt[3]{kr_0})$ [70]. The values of n_1 are listed in Table 3 for different equivalent reflectivity level ε (the maximum relative error between the emulated field and target field) [71].

2.3.2 *Test zone size*

One of the key issues to be addressed in the MPAC setup is how large of a test area can be supported. Test zone characterization [72] has been studied. Many metrics can be used to determine the test zone size, such as field synthesis error and spatial correlation error. It is difficult to define acceptable error thresholds for field synthesis error and spatial correlation error, as these error thresholds cannot be directly reflected in the data rate deviation. Because the throughput can reflect the end-to-end performance of the test system, the throughput error is chosen as the metric to characterize the test zone size. However, in principle, an infinite number of OTA probes are required in the MPAC setup to reproduce the accurate target channel model as a reference for determining the throughput error, which is not feasible. The synthetic MPAC setup (Figure 7) has been proposed to address this challenge [64, 73].

The channel matrix is embedded in the CE in the synthetic MPAC setup, and then the throughput measurement is performed in a conductive manner. During the measurement process, different MPAC configurations and different antenna spacings can be flexibly changed because the MPAC configuration and antenna spacing can be arbitrarily set in (7).

The influence of the user phantom on the test zone size has also been considered [73]. Placing a user phantom in the vicinity of the DUT has two major effects on the MIMO performance. (1) Detuning of the antennas by bulky dielectrics; (2) Blocking and scattering of the incoming waves.

Similarly, the synthetic MPAC setup has also been used [73] for throughput measurements. At the same time, the emulation accuracies of other figures of metrics are also considered, including received power, branch power ratio, and antenna correlation. The results show that the presence of the user phantom near the DUT does not affect the simulation accuracy of the metrics, so the impact of the user phantom on the test zone size is negligible.

2.3.3 *Physical dimension of the setup*

The physical dimension of the setup is determined based on an acceptable error on the amplitude distribution of the spatio-temporal fading when the field strength stability of the system is considered [74]. Other criteria such as power imbalance and correlation error are more directly related to the spatial characteristics of the channel models for determining physical dimensions.

(1) Power imbalance. Considering one probe and free space loss, the Rx power ratio between two

locations on the test area can be written as

$$\Delta P = \frac{L\left(d_1, \lambda\right)}{L\left(d_2, \lambda\right)} = \left(\frac{d_1}{d_2}\right)^2, \tag{26}$$

where d_1 and d_2 are the distances from the probe to the locations on the test area; L is the free space loss, which is defined as

$$L\left(d, \lambda\right) = \left(\frac{4\pi d}{\lambda}\right)^2. \tag{27}$$

When the probe is on the same line with the Rx antennas and the distance between the two Rx antennas is $2r_0$, the maximum power difference can be achieved as

$$\Delta P_{\max} = 10\log_{10}\left(\frac{1 + r_0/R}{1 - r_0/R}\right), \tag{28}$$

where R is the physical dimension of the test setup. The average imbalance can be defined as

$$\Delta P_{\text{aver}} = 10\log_{10}\langle d_{q1,k}^2 / d_{q2,k}^2 \rangle, \tag{29}$$

where q_1, q_2 denote the location pairs of the test area; $\langle\cdot\rangle$ denotes the average operation.

(2) Correlation error. Correlation error is the deviation between the emulated correlation in ideal conditions and the emulated correlation in physically constrained setup, i.e.,

$$E_\rho = \hat{\rho}_{\text{ideal}} - \hat{\rho}_{\text{small}}. \tag{30}$$

Note that the correlation error not only considers field strength stability but also considers phase stability. If we select error thresholds, the physical dimension R can be determined as a function of r_0. A study in [75] described the relationship between R and r_0 as $R = 0.1r_0$ if 0.05 and 0.5 dB are chosen as error thresholds of the root mean square (RMS) of the correlation error and the average power imbalance, respectively.

To save laboratory space and reduce system costs, a small anechoic chamber may be applied. However, the waves illuminating the test area will have curved phase fronts. A plane wave compensation technique has been proposed in small MPAC setups to minimize the spherical effects [76]. It can be seen from (5) that path loss and phase error have important effects on the emulated spatial correlation in a small MPAC setup. The core of the proposed compensation technique is that a far-field probe is emulated by a few near-field probes, and they are connected to different programmable power attenuators and phase shifters but one output of the CE (Figure 8) [76]. The flexible probe setup is used to improve the compensation accuracy, and the particle swarm optimization (PSO) algorithm is adopted to obtain far-field angle locations of the probes.

Suppose there are K far-field probes, each of which uses $\hat{K}$ near-field probes to emulate. Then the channel frequency response (CFR) from the sth Tx antenna to the kth probe of the nth cluster can be written as

$$h_{s,k,n}^{\text{OTA}}\left(t, f\right) = \sqrt{\frac{P_n}{M}} \sum_{\hat{k}=1}^{\hat{K}} \sum_{m=1}^{M} F_s^{\text{Tx}}\left(\varphi_{n,m}\right) g_{k,\hat{k},n} \cdot \exp\left(\text{j}2\pi v_{n,m} t + \text{j}\Phi_{n,m,k}\right) \cdot \exp\left(-\text{j}2\pi f \tau_n\right), \tag{31}$$

where $g_{k,\hat{k},n}$ denotes the complex weight of the $\hat{k}$th near-field probe of the kth far-field probe of the nth cluster. It is demonstrated that this plane compensation technique improves the system performance in terms of field distribution, spatial correlation, and PAS estimation. That is, the conventional far-field criteria can be relieved to implement a small MPAC setup to save costs.

2.3.4 *State-of-art works*

There is still much work to be done to improve the 2D MPAC setup design. For example, the impact of different MS designs and channel models on the test zone size in terms of throughput deviation and the impact of correlation error and power imbalance on DUT performance indicators.

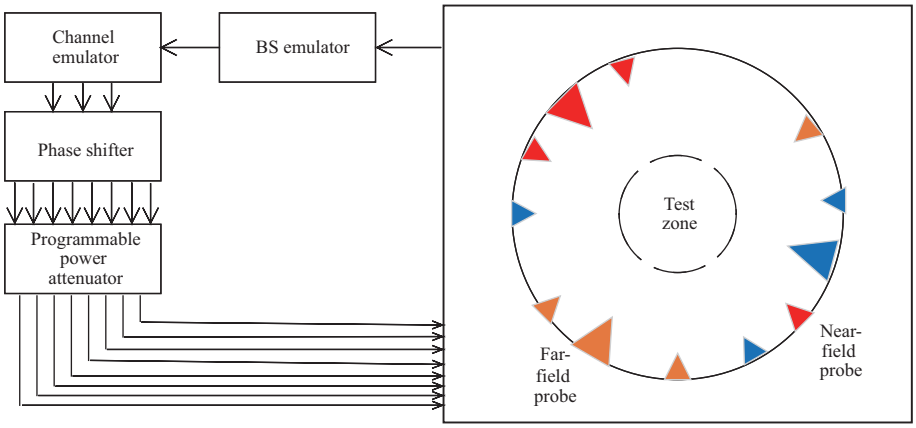

Figure 8 (Color online) MPAC setup involving the plane wave compensation technique.

3 Testing of massive BS in 3D scenario

The use of massive MIMO technology is a promising approach to considerably improve the spectral efficiency of 5G communication systems. The conducted testing is no longer suitable for 5G antenna systems for several reasons. First, 5G antennas are highly integrated units and the number of the antennas will be very large, resulting in unavailable antenna connectors owing to cost, size, and design challenges. Second, 5G antenna systems equipped with possibly hundreds of antennas will need hundreds of RF cable connections and corresponding hardware resources, which is infeasible and costly. Finally, the features of 5G antenna systems rely heavily on their spatial discrimination capability, which cannot be evaluated in a conductive manner [77]. Therefore, MIMO OTA testing is required for 5G antenna systems.

The applicability of the three UE MIMO OTA test methods (i.e., RC, RTS, and MPAC) for massive MIMO BSs can be compared. The RC-based method does not provide angular distribution and cross-polarization discrimination of the channel. Because the millimeter-wave channel is highly sparse and directive, the RC-based method is not suitable for OTA testing of adaptive millimeter-wave antenna systems. Because the RTS method requires measurement of the antenna patterns in the first stage, it is not suitable for dynamic adaptive beamforming systems [78]. Additionally, in the RTS method, the number of OTA antennas should be equal to the number of DUT antennas, resulting in a large number of active OTA antennas.

The MPAC-based method is attractive for massive MIMO BS OTA testing as it is capable of physically simulating the actual multipath environment in an anechoic chamber. The adaptive antenna technology can also be reliably emulated in the MPAC setup. The BS is placed higher and away from scatters, so the AS at the BS side is relatively small. Thus, the PAS is confined in an angular region, making the propagation channel very specular and spare in 5G MIMO communication systems. There is a strong demand to have a new test setup for the OTA testing of 5G BSs. A 3D sectored MPAC setup has been proposed for massive MIMO BS OTA testing [79] to address this challenge. The 3D sectored MPAC setup is more suitable for massive MIMO BS OTA testing for multiple reasons [80]:

(1) The AS at the BS side is small.

(2) The coverage area of the BS antenna array is usually limited to a certain range of angles, such as 60° or 120°.

(3) The sectored MPAC setup can considerably reduce the system cost by reducing the required fading emulators and corresponding hardware resources. Because the DUT is placed at one end of the anechoic chamber, the size of the entire chamber is used.

The hardware resources required by the sectored and uniform MPAC setups to achieve the same correlation error level have been compared [81] (Table 4). The sectored MPAC setup can noticeably reduce the system cost while ensuring the accuracy of the emulation.

This section mainly summarizes channel emulation methods for 3D BS MIMO OTA testing. In addition, a few new metrics are explained to evaluate the accuracy of the channel emulation and requirements for 3D sectored MPAC setup design are also contained in this section.

To ensure that the target channel models are accurately emulated, validation of emulated channel

Table 4 Sectored vs. uniform MPAC hardware required to achieve desired correlation error level

Channel model	SCME UMa	SCME UMi	SCME UMa	SCME UMi
RMS e_ρ	0.1	0.05	0.26	0.09
Sectored MPAC	$K = 12$ (116 m^2)	$K = 16$ (116 m^2)	$K = 12$ (29 m^2)	$K = 16$ (29 m^2)
Uniform MPAC	$K = 60$ (400 m^2)	$K = 100$ (400 m^2)	$K = 60$ (100 m^2)	$K = 100$ (100 m^2)

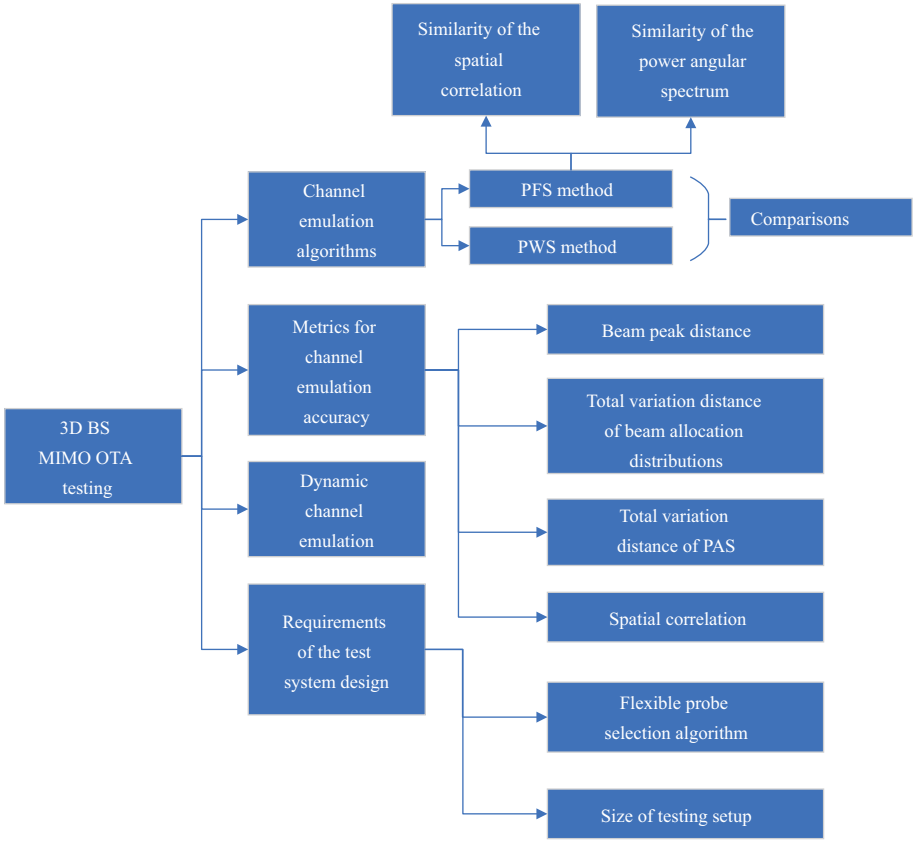

Figure 9 (Color online) Block diagram of Section 3.

models in the sectored MPAC setup is required. The joint angle-delay power profile is selected as the metric for the validation for 5G beamforming management performance. Two estimation algorithms, i.e., the joint angle and delay estimation (JADE) and sequential search algorithm, are considered. It has been concluded that both algorithms provide good estimation accuracies [82]. Notably, the sequential search algorithm provides a little more accuracy and offers lower computation complexity because of the sequential estimation in different domains instead of joint estimation.

Figure 9 draws a block diagram of this section for better illustration.

3.1 Channel emulation algorithms and their comparisons

3.1.1 *Channel emulation algorithms*

Two popular channel emulation algorithms are the PFS method and the PWS method, where the algorithm to obtain the probe weights for the PWS technique is typically similar to the method applied in Subsection 2.1.2, which is omitted here. The idea of the PFS method is mainly to reproduce the spatial characteristics of the target channel at the Rx side by assigning appropriate power weights to the limited active probes in the MPAC setup. The spatial characteristics can be characterized by the spatial correlation or the PAS. So the cost function of the PFS technique also will be the spatial correlation or the PAS.

(1) Similarity of the spatial correlation. First, the DUT needs to be mechanically rotated so that the clusters with higher powers fall within the sector of interest of the BS as many as possible. One study [32] proposed a rotation scheme based on the center gravity of the target PAS. However, this rotation scheme

neglects the effects of weaker clusters, leading to simulation errors. A novel rotation scheme has been proposed in [83] to maximize the total power of the clusters covered by the probe wall.

Next, select the appropriate probes through a switching network. According to the descending order of the cluster powers, each cluster is allocated an active probe that is nearest to the AoA of the cluster until the K probes are allocated. If the number of clusters falling within the sector is less than K, then one should allocate as many probes as possible for the cluster with the highest power, and so on, until the K probes are allocated [32]. Another proposed probe allocation algorithm [83], i.e., the forward allocation (FA) algorithm, has shown better performance. For a pair of spatial locations $q = (\boldsymbol{p}_{q1}, \boldsymbol{p}_{q2})$, the target spatial correlation is defined as

$$\rho_q = \oint P(\Omega)\exp\left(\mathrm{j}\Omega \cdot (\boldsymbol{p}_{q1} - \boldsymbol{p}_{q2})\right) \mathrm{d}\Omega, \tag{32}$$

where Ω denotes the wave vector to the spatial angle Ω; $P(\Omega)$ is the continuous power angle spectrum of the target channel. Because the far-field requirement is usually not met in the massive MIMO BS OTA testing, the emulated spatial correlation in the OTA case should consider the gain and phase errors caused by the spherical waves [84]. The spatial correlation in the OTA case is defined as

$$\hat{\rho}_q = \frac{\sum_{k=1}^{K} g_k L\left(d_{p1,k}\right) L\left(d_{p2,k}\right) \exp\left(\mathrm{j}\|\Omega\|\left(d_{p1,k} - d_{p2,k}\right)\right)}{\sqrt{\sum_{k=1}^{K} L^2\left(d_{p1,k}\right) g_k} \sqrt{\sum_{k=1}^{K} L^2\left(d_{p2,k}\right) g_k}}, \tag{33}$$

where g_k is the power weight of the kth active OTA probe and $\|\Omega\| = \frac{2\pi}{\lambda}$; $L\left(d_{p1,k}\right)$ and $L\left(d_{p2,k}\right)$ are the path loss terms of the positions p_1 and p_2 to the kth probe, respectively.

$$L\left(d_{p1,k}\right) = \frac{4\pi d_{p1,k}}{\lambda}. \tag{34}$$

The power weights of the probes can then be obtained by solving the following objective function:

$$\boldsymbol{G} = \operatorname{argmin} \sum_{q=1}^{Q} |\rho_q - \hat{\rho}_q|^2. \tag{35}$$

(2) Similarity of the PAS [85]. Nevertheless, the spatial correlation may be a less relevant metric for massive MIMO OTA testing. There are mainly two reasons: (i) Different PASs may yield similar spatial correlations due to limited spatial samplings; (ii) Compared with the reconstructed spatial correlation, the reconstructed PAS can more intuitively reflect the beamforming features, such as beam acquisition and tracking, which are essential in massive MIMO.

The PAS can be obtained from the Barlett beamforming algorithm, which calculates the angle by measuring the signal power at each possible AoA and selecting the maximum power direction as the estimate of the AoA. The target PAS estimate can be written as

$$p(\Omega) = a^{\mathrm{H}}(\Omega)\boldsymbol{R}a(\Omega), \tag{36}$$

where $a(\Omega)$ is the steering vector of the DUT to the spatial angle Ω; $\boldsymbol{R}$ is the target channel spatial correlation matrix, whose element is ρ_q. For emulated channels in the chamber, the PAS estimate can be written as

$$\hat{p}(\Omega) = a^{\mathrm{H}}(\Omega)\hat{\boldsymbol{R}}a(\Omega), \tag{37}$$

where $\hat{\boldsymbol{R}}$ is the emulated channel spatial correlation matrix, whose element is $\hat{\rho}_q$. Therefore, the objective function can be written as

$$\min_{\boldsymbol{G}} \|\boldsymbol{p} - \hat{\boldsymbol{p}}\|_2^2 \quad \text{s.t. } \|\boldsymbol{G}\| = 1, 0 \leqslant g_k \leqslant 1, \tag{38}$$

where $\boldsymbol{p}$ and $\hat{\boldsymbol{p}}$ represent the target and emulated PAS matrices, respectively. According to the obtained OTA antenna power weights, the channel matrix of the emulated channel can be written as [86]

$$h_{s,k,n}^{\mathrm{OTA}}(f,t) = \sqrt{\frac{P_n}{M}} \sum_{m=1}^{M} f_s^{\mathrm{Tx}}\left(\Omega_{n,m}^{\mathrm{Tx}}\right) w_{n,m,k} \times \exp\left(\frac{\mathrm{j}2\pi \hat{r}_{s,n,m} \cdot \boldsymbol{d}_{tx,s}}{\lambda}\right)$$

$$\times \exp\left(\mathrm{j}2\pi v_{n,m}t + \mathrm{j}\Phi_{n,m,k} - \mathrm{j}2\pi f\tau_n\right), \tag{39}$$

$$\hat{h}_{u,s,n}(f,t) = \sum_{k=1}^{K} f^{\mathrm{OTA}}\left(\Omega_{n,k}^{\mathrm{OTA}}\right) f_u^{\mathrm{Rx}}\left(\Omega_{n,k}^{\mathrm{OTA}}\right) \alpha_{k,u} h_{s,k,n}^{\mathrm{OTA}}(f,t), \tag{40}$$

where $\Omega_{n,m}^{\mathrm{Tx}}$ is the solid AoD of the mth subpath of the nth cluster; $w_{n,m,k}$ is the amplitude weights of the kth probe of the mth subpath of the nth cluster; K is the number of the active probes; $\hat{r}_{s,n,m}$ is the spherical unit vector corresponding to the AoD of the mth subpath of the nth cluster; $\boldsymbol{d}_{tx,s}$ is the location vector of the sth transmit antenna element; $\cdot$ denotes the dot product operator; f^{OTA} is the OTA antenna pattern; $\Omega_{n,k}$ is the solid AoA of the kth probe of the nth cluster; $\alpha_{k,u}$ is the propagation coefficient from the kth probe antenna to the uth DUT antenna element.

3.1.2 *Comparisons of channel emulation algorithms*

This subsection mainly provides comparisons of channel emulation algorithms listed in Subsection 3.1.1.

(1) Comparison between two PFS methods. The comparison between the two PFS methods described above is illustrated in [85]. The target channel is a channel with a single cluster, which follows the truncated Laplacian distribution. The mean azimuth and elevation of the arrival of the cluster are 20° and −15°, respectively. The azimuth spread of arrival (ASA) and elevation spread of arrival (ESA) are set to 10° and 3°, respectively.

Two metrics are used to evaluate the emulation accuracy. The first is the deviation between the peaks of the target and emulated PASs, which is defined as the logarithm of the ratio of the simulated PAS peak to the target PAS peak. The closer this metric is to 0, the better the simulation accuracy. The other metric is the RMS emulation error of PASs, which is defined as $\sqrt{\frac{1}{N}\|\boldsymbol{p}-\hat{\boldsymbol{p}}\|_2^2}$, where N is the number of PASs in $\boldsymbol{p}$.

The deviations between the peaks of the target and emulated PASs based on the spatial correlation optimization and PAS optimization are −0.951 and −1.701 dB, respectively. The RMS emulation errors of PASs based on the spatial correlation optimization and PAS optimization are 1.239 and 1.635 W, respectively. It can be seen that the PFS method with the PAS similarity as the cost function has higher emulation accuracy in terms of reconstructed PASs.

(2) Comparison between PFS and PWS methods. Some studies [87, 88] have noted that for massive MIMO and high-frequency scenarios, the field synthesis method requires more probe antennas to achieve a sufficiently accurate emulation. Moreover, for the upcoming 5G communication system, phase calibration of the BS OTA testing is difficult owing to the non-linearity of the RF components such as the switching network and power amplifiers.

In order to compare the emulation accuracies of the PFS and PWS methods, the 3GPP CDL model is used as the target channel model. Assume that there are $Q = 629$ available probes to form a sectored probe wall, where the azimuth angle occupies 135° and the elevation angle occupies 60°. The angular resolution of the probes is 3.75°. Sixteen active probes are selected by the probe selection method as illustrated in Subsection 3.1.1 for the emulation. The DUT is an 8×8 uniform rectangular array with 0.5λ element spacing. The distance from the center of the DUT to the probe panel is 2 m, and the center frequency is 28 GHz.

Figure 10 illustrates the estimated PASs of the target channel, and the emulated channels using the PFS and PWS methods [86]. The abscissa and ordinate represent the azimuth and elevation angles, respectively, and the color represents the power level. The total variation distance of PAS is used as the performance metric to evaluate the channel emulation accuracy. The definition of the total variation distance of the PAS will be described in detail in Subsection 3.2. The results show that the total variation distance calculated by the PFS and PWS methods are 8.5% and 9.76%, respectively. The subfigures in Figure 10 look like almost the same because the emulation accuracy is high. Nevertheless, it can be seen that the emulation error using the PFS technique is less than the PWS technique. Therefore, it is confirmed that the PFS method is more suitable for 3D sectored MPAC OTA testing.

This finding may be surprising given the fact that the PWS method outperforms the PFS method for 2D MPAC tests. In theory, the PWS method ought to be more accurate than the PFS method (at the expense of higher complexity) provided that all the probes can be connected to the CE. For 3D sectored MPAC testing, however, this implies a formidable system cost. In order to keep the system cost to an acceptable level, only a few probes are selected to be connected to the CE (for a specific target

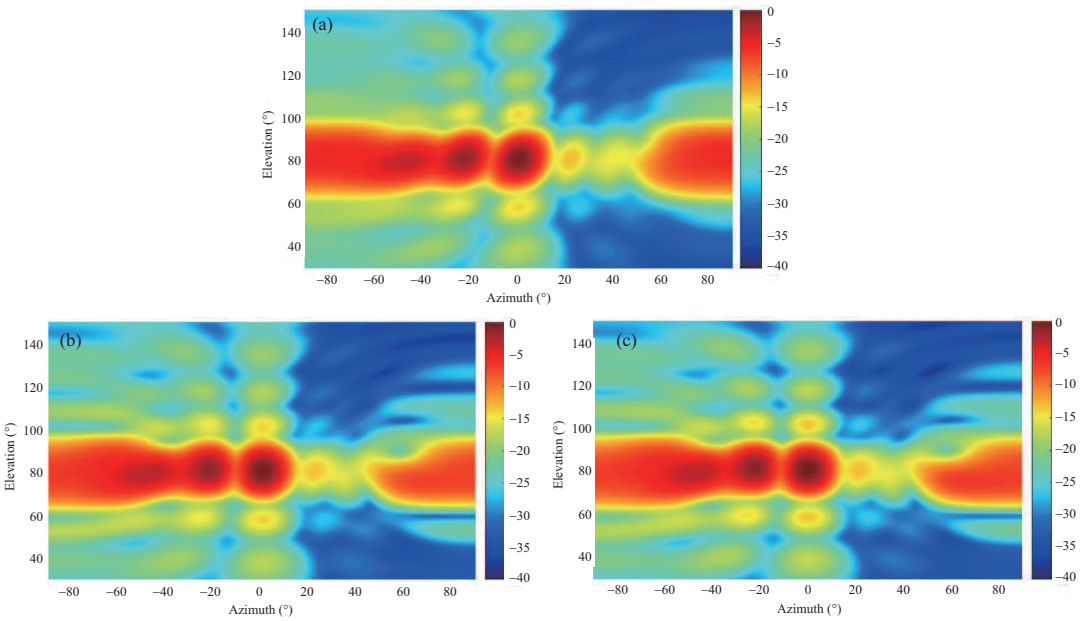

Figure 10 (Color online) Estimated PASs of (a) the target channel, (b) the emulated channel using PFS technique, and (c) the emulated channel using PWS technique.

channel) [78]. In this case, the PFS method outperforms the PWS method because the PFS method is more robust to the sampling errors in the case of limited probes.

3.2 Channel emulation accuracy

New metrics are needed to evaluate the performance of millimeter-wave terminals and adaptive antenna systems [32, 89]. The PAS-based metrics (i.e., PAS estimation and spatial correlation) can be adopted to evaluate 4G antenna systems. Furthermore, two additional metrics about beam probability are considered for 5G antenna systems.

(1) Beam peak distance. This metric and the next one assume that the DUT utilizes fixed beams with a code book of discrete antenna weights. By scanning all beam powers in turn, the beam with the highest power among all fixed beams is selected at each moment. In NLOS scenarios, fading disperses the probability distribution. In LOS scenarios, especially in the case of the high Ricean K-factor, the beam in the LOS direction always has the highest power.

Beam peak distance is the angular distance between probability weighted average directions of the allocated beams. It is defined as

$$D_b = \left\| \sum_{b=1}^{B} \Omega_b p_r(\Omega_b) - \Omega_b p_o(\Omega_b) \right\|, \tag{41}$$

where Ω_b denotes the spatial angle of the bth beam; $p_r(\Omega_b)$ and $p_o(\Omega_b)$ denote the probability of detecting the maximum power in the bth beam for the target and OTA case, respectively [90].

(2) Total variation distance of beam allocation distributions. This metric is another beam selection metric, and the data required for the calculation is the same as the beam peak distance. The total variation distance of beam allocation distributions is defined as

$$D_s = \sum_{b} \frac{|p_r(\Omega_b) - p_o(\Omega_b)|}{2}. \tag{42}$$

The range of D_s is $[0, 1]$, where 0 represents complete similarity and 1 represents complete dissimilarity.

(3) Total variation distance of PAS. This metric and the next one are both used to measure the ability of OTA testing to reconstruct PASs. First, the PASs are estimated by the Bartlett beamforming, using (36) and (37). This actually means filtering the PAS of the channel using the aperture of the DUT array.

Then, normalize the PAS estimates of the target and emulated channels so that they can be used as probability density functions. Finally, the total variation distance of the PAS is defined as

$$D_p = \frac{1}{2}\int \left| \frac{\hat{P}_r(\Omega)}{\int \hat{P}_r(\Omega')\,\mathrm{d}\Omega'} - \frac{\hat{P}_o(\Omega)}{\int \hat{P}_o(\Omega')\,\mathrm{d}\Omega'} \right| \mathrm{d}\Omega, \tag{43}$$

where $\hat{P}_r(\Omega)$ and $\hat{P}_o(\Omega)$ are the PAS estimates of the reference channel and emulated channel, respectively. The similarity between the target and the simulated beamforming power patterns can be defined as [91]

$$S = (1 - D_p) \times 100\%. \tag{44}$$

The range of S is [0,1], where 0 means completely dissimilar and 1 means completely similar.

(4) Spatial correlation error. The purpose of this metric is to assess the deviation of the spatial correlation between the target and the emulation case, which indicates the accuracy of the PAS simulation. The weighted RMS spatial correlation error is defined as

$$e_\rho = \sqrt{\frac{1}{Q}\sum_{q=1}^{Q} |\rho_q - \hat{\rho}_q|^2 \max(|\rho_q|, |\hat{\rho}_q|)}, \tag{45}$$

where ρ_q and $\hat{\rho}_q$ represent the spatial correlations of the position pair $q = (\boldsymbol{p}_{q1}, \boldsymbol{p}_{q2})$ of the target and emulated channels, respectively. Q represents the number of the total position pairs. The correlation deviation is weighted by the corresponding correlation level. It can be seen that the effect of the error of the small spatial correlation is not very important.

For OTA metrics, when the DUT size is fixed, an increase in the number of OTA probes should improve the simulation accuracy, because channels simulated by more OTA probes will be closer to the target channels. On the other hand, when the number of probes is fixed, an increase in the size of the DUT should reduce the simulation accuracy, because a DUT with a higher beam resolution is easier to distinguish target and simulated channels. However, the beam peak distance does not follow this principle, which is demonstrated in [92]. Therefore, the beam peak distance is not suitable for studying the relationship between the size of the test area and the number of OTA probes.

3.3 Emulation of dynamic radio channel

It is important to evaluate massive MIMO devices under dynamic channel conditions because of the following reasons [93]:

(1) Hybrid beamforming is significant in the millimeter band, which will cause the channel to become highly dynamic.

(2) The link distance is short at the millimeter-wave frequency, so even a short distance of the movement can cause a change in the channel spatial structure.

(3) The propagation is very sensitive to obstacles, which results in rapid changes in power levels observed by different multipath components.

Because the channel is dynamic (i.e., time varying), the PAS is also time varying, which requires the selection of the active antenna probes and the weights of the antenna probes to be updated in real time as the channel changes. Considering that the probe weights optimization method in Subsection 3.1 is computational in the case of dynamic channels, an efficient and simple computational method has been proposed. This approach is based on minimizing the target PAS and the reconstructed PAS in the OTA case. First, form a steering vector matrix from the DUT array to the OTA probe directions, i.e., $\boldsymbol{A} = [\boldsymbol{a}(\Omega_1) \cdots \boldsymbol{a}(\Omega_K)] \in \mathbb{C}^{M\times K}$.

Similar to (36), the PAS estimate defined to the K probe directions is defined as

$$\hat{\boldsymbol{P}}_o = \boldsymbol{A}^{\mathrm{H}}\boldsymbol{R}\boldsymbol{A} \in^{K\times K} . \tag{46}$$

Then the power weight vector can be obtained by

$$\boldsymbol{W} = \left|\mathrm{diag}(\hat{\boldsymbol{P}}_o)\right| \in \mathbb{R}^{K\times 1}, \tag{47}$$

where $\mathrm{diag}(\boldsymbol{P})$ represents a column vector consisting of the diagonal elements in the matrix $\boldsymbol{P}$.

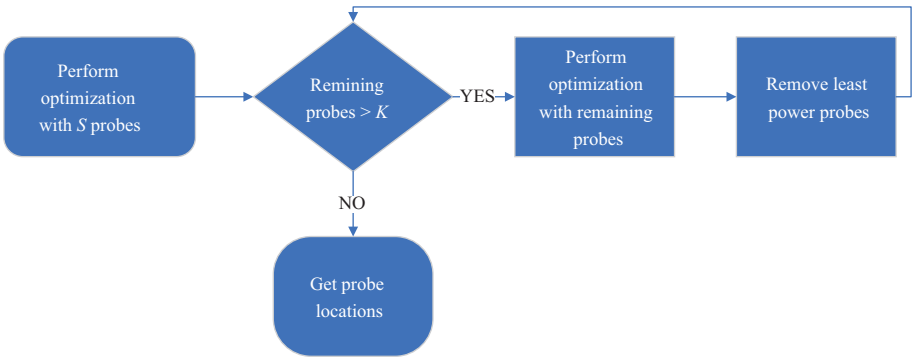

Figure 11 (Color online) Flowchart of the multishot algorithm.

This simple weights calculation method greatly reduces the computational complexity because no numerical optimization is involved in the calculation process. The findings in [93, 94] have proven the feasibility of this approach.

3.4 Rrequirements of the 3D BS test system design

3.4.1 *Flexible probe selection algorithm*

The probe selection procedure can be regarded as a combinatorial optimization problem. Traverse all the combinations to obtain the global optimal solution. However, due to the huge number of available probes in the massive MIMO OTA test setup, the large number of combinations make this method infeasible. To improve the efficiency and enhance the emulation accuracy, a few flexible probe selection algorithms including multishot, artificial bee colony (ABC), and PSO have been proposed.

(1) Multishot algorithm [34, 95]. The purpose of the multishot algorithm is to remove several probes with the least contribution after each iteration until all the K probes are retained (Figure 11) [95].

(2) ABC algorithm [95]. The ABC algorithm is an optimization method proposed by imitating bee behavior (Figure 12) [95]. It only needs to compare the advantages and disadvantages of the problem without understanding the special information of the problem, and the global optimal value would emerge by local optimization behavior of individual artificial bees. The ABC algorithm provides a faster convergence speed than the other algorithms.

(3) PSO algorithm [76, 96]. The PSO algorithm mimics the clustering behavior of insects, herds, and birds (Figure 13) [96]. These groups look for food in a collaborative way, and each member of the group continually changes its search model by learning and observing the experience of other members. The core of the PSO algorithm is the speed and position update principle.

It is demonstrated in [96] that the PSO algorithm can reduce the number of probes while improving the simulation accuracy. The simulation results in [95] show that when the number of probes is sufficient, the multishot algorithm can almost obtain the global optimal solution. However, when the number of probes is limited, the performance of the algorithm needs to be improved. The ABC algorithm is superior to the multishot algorithm when the number of active probes is limited.

3.4.2 *Size of testing setup*

Studies in [97, 98] have evaluated the measurement distance of the massive MIMO BS in the radiated OTA test setup (i.e., the distance R from the probe to the center of the test area). The study in [98] focuses on the frequency of 28 GHz, whereas Ref. [97] aims to determine whether the traditional far-field criteria must be followed when determining the measurement range. The link budget analyses for 2.6 and 3.5 GHz are based on the current LTE parameters. For the downlink, the power at the input of the UE emulator can be written in dB as

$$P_E = P_{\mathrm{TX,BS}} + G_{\mathrm{TX}} - 10\log_{10}\left[\left(\frac{4\pi R f_c}{\mathrm{c}}\right)^2\right] + G_P + G_c + G_{\mathrm{CE}}, \tag{48}$$

where $P_{\mathrm{TX,BS}}$ denotes the Tx power of the BS; G_{TX} denotes the BS antenna gain; R is the measurement range; c is the speed of light; f_c is the center frequency; G_P is the probe antenna gain; G_c is the OTA cable loss and G_{CE} is the CE gain.

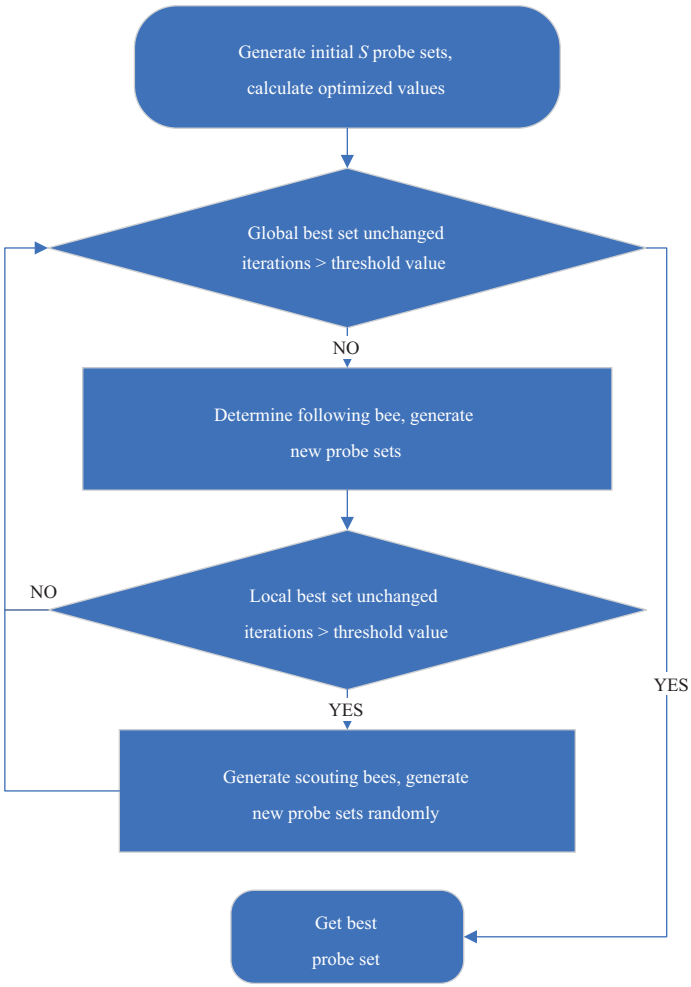

Figure 12 (Color online) Flowchart of the ABC algorithm.

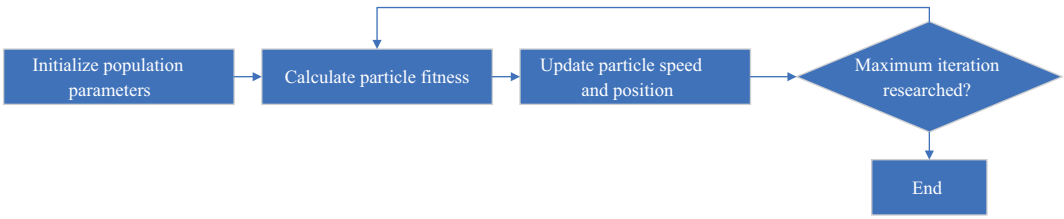

Figure 13 (Color online) Flowchart of the PSO algorithm.

The power at the BS input can be similarly written according to (48) for uplink transmission. Because the transmit power of the UE is much smaller than that of the BS, the UE has stricter requirements on the power link budget. For the uplink, the −90 dBm energy per resource element is used as the target. Therefore, it is concluded that the maximum R of 2.6 GHz is 5 m, and the maximum R of 3.5 GHz is 3.5 m. Of course, the link budget analysis presented here is only an approximation, because only one BS and one probe are considered in the analysis.

Field performance analyses (e.g., amplitude error, angular error, and phase error) at different frequencies (e.g., 2.6, 3.5, and 28 GHz) indicate that the demand for R decreases as the frequency increases. In the DoA simulation accuracy analysis, the beamforming algorithm, which is insensitive to error, is used to verify that the DoA can be well estimated even if the far-field distance is not satisfied.

Multi-user MIMO (MU-MIMO) sum rate capacity is another important metric for evaluating OTA setup measurement distance for high and low frequencies. For the high frequency such as 28 GHz, the MU-MIMO sum rate capacity is presupposed to be full degrees of freedom in combining elements of the

BS array. Several UEs can be randomly selected as a subset for each simulation, and the simulation can be repeated for many (e.g., hundreds) random UE subsets. By a sub-optimal linear precoding method (e.g., forcing zero), the linear precoding vectors can be determined for each UE as

$$\boldsymbol{W}(t) = \boldsymbol{H}^{\mathrm{H}}(t)\left(\boldsymbol{H}(t)\boldsymbol{H}^{\mathrm{H}}(t)\right)^{-1}, \tag{49}$$

where $\boldsymbol{H}(t)$ is the composite channel transmission matrix for one UE subset and all BS elements; $\boldsymbol{w}_k(t)$ represents the kth row of $\boldsymbol{W}(t)$. Then, the sum rate capacity can be calculated as

$$C(t) = \sum_{k=1}^{K} 1\log_2\left(1 + \frac{\gamma}{K}\left|\boldsymbol{w}_k(t)\boldsymbol{h}_k(t)\right|^2\right), \tag{50}$$

where γ is the signal to noise ratio and $\boldsymbol{h}_k(t)$ is the kth column vector of $\boldsymbol{H}(t)$. The simulation results show that even if the measurement distance R is smaller than the far-field criteria, the error of MU-MIMO sum rate capacity is insignificant compared to that of the far field case ($R = 1000$ m).

Another important metric called fixed beam power loss for the 28 GHz evaluation has been proposed [98]. It is necessary to assume that the communication system has fixed beams, that is, with a discrete code book of BS antenna weights. The BS array can at least partially use analog beamforming to compose beams into a pre-defined set of directions. The loss in the kth probe direction can be expressed as follows:

$$Q_k = \left|\frac{1}{M}\sum_{m=1}^{M}\cos\left(\beta_{k,m} - \alpha_{k,m}\right)\right|^2, \tag{51}$$

where $\alpha_{k,m}$ is the spherical wave phase error from the kth probe to the mth DUT element with respect to the phase in the origin. $\alpha_{k,m}$ is defined as

$$\alpha_{k,m} = \frac{2\pi}{\lambda}\left(\|\boldsymbol{a}_k - \boldsymbol{b}_m\| - R\right), \tag{52}$$

where $\boldsymbol{a}_k$ represents the position vector of the kth probe; $\boldsymbol{b}_m$ represents the position vector of the mth DUT element. $\beta_{k,m}$ is the phase error of the kth probe direction for a planar wavefront and can be calculated as

$$\beta_{k,m} = \frac{-\boldsymbol{a}_k}{\|\boldsymbol{a}_k\|}\cdot\boldsymbol{b}_m\frac{2\pi}{\lambda}. \tag{53}$$

Then, the average fixed beam power loss of the K probe locations can be calculated as

$$Q_{\mathrm{av}} = \frac{1}{K}\sum_{k=1}^{K} Q_k. \tag{54}$$

If the acceptable error threshold is assumed to be 2 dB, then the relationship between the maximum dimension D and measurement distance R can be approximated as a linear function $R = 14.46D - 1.1$. If the BS is assumed to be a 20×20 planar array and the element spacing is 0.5λ, then the minimum value of R can be approximated to be 0.85 m [98].

It can be seen from the above analysis that for the massive MIMO BS OTA testing, the measurement distance R does not necessarily have to meet the far-field criteria, and the far-field requirement can be appropriately relieved [97].

4 New testing methods for 5G radios

4.1 5G massive virtual testing

The installation of the practical anechoic chamber, the probe plane, and the implementation of the switching circuit can be complex and costly for the 3D sectored MPAC OTA test setup. Thus, a virtual OTA testing method has been proposed, and the concept of the flexible virtual probe has been adopted. The main idea of this method is to replace the anechoic chamber, probe plane, and switching circuit with

a phase matrix [99]. The probe selection method is the same as that proposed in Subsection 3.1, and the phase matrix can be written as

$$\boldsymbol{F} = \{f_{m,k} = \mathrm{e}^{\mathrm{j}\frac{2\pi}{\lambda}\boldsymbol{r}_m \cdot \hat{\boldsymbol{\Omega}}_k}\}, \tag{55}$$

where $\boldsymbol{r}_m$ is the unit vector of the mth DUT element and $\hat{\boldsymbol{\Omega}}_k$ is the unit position vector of the solid angle of the kth probe.

The feasibility of this method has been verified by three metrics, including spatial correlation error, total variation distance of PAS, and beam statistic distance [99].

4.2 New method based on reflective properties of concave surfaces

The proposed method in [100] can generate highly dynamic 3D environments by making use of reflective properties of concave surfaces (ellipsoid and elliptical cylinder reflectors) to emulate real-life millimeter-wave channel propagation scenarios.

The test setup comprises an ellipsoid of revolution or a set of elliptical cylinder reflectors, a feeder antenna, a DUT, and a BS emulator. The feeder antenna should be an array antenna that can generate multiple simultaneous independent beams. The DUT and feeder antenna are placed at different focal points. The ray emanated from one focal point will arrive at another focal point. Initial test results have been described in [100], implemented with an elliptical cylinder reflector. This testing system enjoys lower cost at the expanse of reduced flexibility in channel emulations.

5 Conclusion and future work

This review discussed various technical points of MIMO OTA testing in the anechoic chamber setup. The channel emulation methods, including PFS, PWS, and EIV methods in 2D UE MIMO OTA testing and PFS and PWS methods in 3D BS MIMO OTA testing are presented. Some key aspects of the MPAC setup are also studied, such as test zone size, the physical dimension of the setup, and the number of probes. Two measurement setups are introduced in this paper, i.e., a 2D uniform MPAC setup and a 3D sectored MPAC setup. The 3D sectored MPAC setup is proposed to accurately reproduce the desired propagation channels, while the cost of the setup can be significantly reduced in the massive MIMO BS antennas OTA testing. The setup is cost-effective mainly because the corresponding hardware resources are reduced. For example, the active probes are reduced by the switching circuits, and the DUT is placed on one side of the anechoic chamber to reduce the chamber size. Some novel massive test methods are also included in this paper. Future research should focus on new techniques and algorithms to save costs related to the MPAC setups. In addition, the active probes selection algorithm with lower computational complexity, the definition of the mmWave channel emulation metrics error threshold, and the calibration of the mmWave test system all require further investigations.

Acknowledgements This work was supported in part by National Key Research and Development Program of China (Grant No. 2020YFA0709800), National Natural Science Foundation of China (Grant Nos. 62171362, 61801366, 81701774, 61771423), Natural Science Foundation of Shaanxi Province (Grant No. 2020JM-078), National Key Research and Development Program of China (Grant No. 2018YFA0701400), Zhejiang Lab (Grant No. 2018EB0ZX01), Key-Area Research and Development Program of Guangdong Province (Grant No. 2018B030333001), and Fundamental Research Funds for the Central Universities (Grant No. 2019XZZX003-20).

References

1 You X H, Wang C X, Huang J, et al. Towards 6G wireless communication networks: vision, enabling technologies, and new paradigm shifts. Sci China Inf Sci, 2021, 64: 110301
2 Yuan Y F, Zhao Y J, Zong B Q, et al. Potential key technologies for 6G mobile communications. Sci China Inf Sci, 2020, 63: 183301
3 He R, Ai B, Wang G, et al. Wireless channel sparsity: measurement, analysis, and exploitation in estimation. IEEE Wirel Commun, 2021. doi: 10.1109/MWC.001.2000378
4 3GPP. User equipment (UE)/mobile station (MS) over the air (OTA) antenna performance; conformance testing (release 9). 3GPP TS 34.114, 2009. http://www.arib.or.jp/english/html/overview/doc/STD-T63v9_20/2_T63/ARIB-STD-T63/Rel9/34/A34114-920.pdf
5 CTIA Certification. Test plan for mobile station over the air performance. Method of measurement for radiated RF power and receiver performance. Revision Number 2.2.2, 2008. https://api.ctia.org/docs/default-source/default-document-library/ctia-test-plan-for-mobile-station-over-the-air-performance-revision-3-1.pdf
6 Obayashi S, Ohishi T, Karasawa Y. Effect of vertical angle spread of propagation channel on MIMO OTA measurement method. In: Proceedings of Asia-Pacific Microwave Conference, Yokohama, 2010. 1934–1937

7 Rumney M, Pirkl R, Landmann M H, et al. MIMO over-the-air research, development, and testing. Int J Antenn Propag, 2012, 2012: 1–8
8 Jing Y, Zhao X, Kong H W, et al. Two-stage over-the-air (OTA) test method for LTE MIMO device performance evaluation. Int J Antenn Propag, 2012, 2012: 1–6
9 Kyösti P, Jämsä T, Nuutinen J P. Channel modelling for multiprobe over-the-air MIMO testing. Int J Antenn Propag, 2012, 2012: 1–11
10 Arsalane N, Mouhamadou M, Decroze C, et al. 3GPP channel model emulation with analysis of MIMO-LTE performances in reverberation chamber. Int J Antenn Propag, 2012, 2012: 1–8
11 Kildal P S, Rosengren K. Correlation and capacity of MIMO systems and mutual coupling, radiation efficiency, and diversity gain of their antennas: simulations and measurements in a reverberation chamber. IEEE Commun Mag, 2004, 42: 104–112
12 Chen X M, Xue W, Shi H, et al. Orbital angular momentum multiplexing in highly reverberant environments. IEEE Microw Wirel Compon Lett, 2020, 30: 112–115
13 Chen X M. Throughput modeling and measurement in an isotropic-scattering reverberation chamber. IEEE Trans Antenn Propag, 2014, 62: 2130–2139
14 Yu W, Qi Y H, Liu K F, et al. Radiated two-stage method for LTE MIMO user equipment performance evaluation. IEEE Trans Electromagn Compat, 2014, 56: 1691–1696
15 Fan W, Kyosti P, Hentila L, et al. MIMO terminal performance evaluation with a novel wireless cable method. IEEE Trans Antenn Propag, 2017, 65: 4803–4814
16 Toivanen J T, Laitinen T A, Kolmonen V M, et al. Reproduction of arbitrary multipath environments in laboratory conditions. IEEE Trans Instrum Meas, 2011, 60: 275–281
17 Sharma R K, Kotterman W, Landmann M H, et al. Over-the-air testing of cognitive radio nodes in a virtual electromagnetic environment. Int J Antenn Propag, 2013, 2013: 1–16
18 Khatun A, Kolmonen V M, Hovinen V, et al. Experimental verification of a plane-wave field synthesis technique for MIMO OTA antenna testing. IEEE Trans Antenn Propag, 2016, 64: 3141–3150
19 Llorente I C, Fan W, Nielsen J O, et al. Comparison of channel emulation techniques in multiprobe anechoic chamber setups. In: Proceedings of the 9th European Conference on Antennas and Propagation (EuCAP), Lisbon, 2015
20 Fan W, Carreno X, Kyosti P, et al. Over-the-air testing of MIMO-capable terminals: evaluation of multiple-antenna systems in realistic multipath propagation environments using an OTA method. IEEE Veh Technol Mag, 2015, 10: 38–46
21 Mow M A, Niu B L, Schlub R W, et al. Tools for design and analysis of over-the-air test systems with channel model emulation capabilities. US Patent, 20 110 270 567, 2011
22 Kyösti P, Nuutinen J. Over the air test. US Patent, 20 110 189962, 2011
23 Reed J D. Emulation and controlled testing of MIMO OTA channels. US Patent 20 110 299 570, 2011
24 Fan W, Nielsen J Ø, Franek O, et al. Antenna pattern impact on MIMO OTA testing. IEEE Trans Antenn Propag, 2013, 61: 5714–5723
25 Almers P, Bonek E, Burr A, et al. Survey of channel and radio propagation models for wireless MIMO systems. Eurasip J Wirel Commun Netw, 2007, 2007: 019070
26 Baum D S, Hansen J, Salo J, et al. An interim channel model for beyond-3G systems: extending the 3GPP spatial channel model (SCM). In: Proceedings of the 61st Vehicular Technology Conference, Stockholm, 2005. 3132–3136
27 Kyösti P, Meinilö J, Hentilö L, et al. IST-4-027756 WINNER II D1.1.2 V1.0 WINNER II Channel Models. IST-WINNER II Technical Report. 2007
28 3GPP. Study on cannel model for frequencies from 0.5 to 100 GHz. 3GPP TR 38.901, 2017
29 Wu X F, Wang N, Zhang Z H, et al. Comparison tests and hand phantom standardization for multi-probe based MIMO OTA. In: Proceedings of the 5th Asia-Pacific Conference on Antennas and Propagation (APCAP), Taiwan, 2016. 321–322
30 Carreño X, Fan W, Nielsen J O, et al. Test setup for anechoic room based MIMO OTA testing of LTE terminals. In: Proceedings of the 7th European Conference on Antennas and Propagation (EuCAP), Gothenburg, 2013. 1417–1420
31 CTIA Certification. Test plan for 2×2 downlink MIMO and transmit diversity over-the air performance. Technical Report Version 1.1, 2016
32 Kyosti P, Hentila L, Fan W, et al. On radiated performance evaluation of massive MIMO devices in multiprobe anechoic chamber OTA setups. IEEE Trans Antenn Propag, 2018, 66: 5485–5497
33 Kyösti P, Khatun A. Probe configurations for 3-D MIMO over-the-air testing. In: Proceedings of the 7th European Conference on Antennas and Propagation (EuCAP), Gothenburg, 2013. 1421–1425
34 Weimin W M, Li M Y, Liu Y A, et al. Novel physical probe configurations in a multi-probe based 3D MIMO OTA setup. J China Univ Post TeleCommun, 2017, 24: 60–66
35 Wang R R, Wang W M, Wu Y G, et al. 3D channel spatial characteristic emulation in multi-probe anechoic chamber setups. In: Proceedings of Global Wireless Summit (GWS), Chiang Rai, 2018. 348–353
36 Yuan Y, Wang W M, Liu Y N, et al. Impact of probe ring location on test area performance in 3D MIMO OTA setup. In: Proceedings of the 11th International Symposium on Antennas, Propagation and EM Theory (ISAPE), Guilin, 2016. 858–861
37 Zhang Z, Tian L, Zhang J H, et al. Analysis of test volume size in 3D MIMO OTA for 5G. In: Proceedings of IEEE International Conference on Communications Workshops (ICC Workshops), Shanghai, 2019
38 Fan W, Sun F, Nielsen J Ø, et al. Probe selection in multiprobe OTA setups. IEEE Trans Antenn Propag, 2014, 62: 2109–2120
39 Yang X L, Zhang P, Chen J Q, et al. Probe subset selection in 3D multiprobe OTA setup. In: Proceedings of the 29th Annual International Symposium on Personal, Indoor and Mobile Radio Communications (PIMRC), Bologna, 2018
40 Fan W, Szini I, Nielsen J Ø, et al. Channel spatial correlation reconstruction in flexible multiprobe setups. Antenn Wirel Propag Lett, 2013, 12: 1724–1727
41 Gao H Q, Wang W M, Wu Y L, et al. 3D flexible multi-probe setups for MIMO OTA testing. In: Proceedings of the 5th International Symposium on Electromagnetic Compatibility, Beijing, 2017
42 Wang W M, Wang R R, Gao H Q, et al. Implementation and analysis of 3D channel emulation method in multi-probe anechoic chamber setups. IEEE Access, 2019, 7: 108571

43 Fan W, Kyösti P, Nuutinen J P, et al. On probe weighting for MIMO OTA testing in anechoic chamber setups. In: Proceedings of Asia-Pacific Microwave Conference (APMC), Nanjing, 2015
44 Belhabib M, D'Errico R, Bernard U. Effect of finite ring radius and antenna radiation on spatial correlation in multiprobe over-the-air tests. In: Proceedings of the 10th European Conference on Antennas and Propagation (EuCAP), Davos, 2016
45 Belhabib M, D'Errico R, Uguen B. Spatial correlation in spherical and cylindrical 3D MIMO over-the-air tests setups. In: Proceedings of the 10th European Conference on Antennas and Propagation (EuCAP), Davos, 2016
46 Fan W, Szini I, Foegelle M D, et al. Measurement uncertainty investigation in the multi-probe OTA setups. In: Proceedings of the 8th European Conference on Antennas and Propagation (EuCAP), Hague, 2014. 1068–1072
47 Foged L J, Scannavini A, Gross N, et al. MIMO OTA testing using a multiprobe system approach. In: Proceedings of the 7th European Conference on Antennas and Propagation (EuCAP), Gothenburg, 2013. 1673–1677
48 Guo L, Sun C, An X D, et al. Over the air MIMO channel model validation. In: Proceedings of the 7th European Conference on Antennas and Propagation (EuCAP), Gothenburg, 2013. 1848–1852
49 Fan W, Nielsen J Ø, Carreño X, et al. Impact of system non-idealities on spatial correlation emulation in a multi-probe based MIMO OTA setup. In: Proceedings of the 7th European Conference on Antennas and Propagation (EuCAP), Gothenburg, 2013. 1663–1667
50 Fan W, Nielsen J Ø, Carreño X, et al. Impact of probe placement error on MIMO OTA test zone performance. In: Proceedings of Loughborough Antennas and Propagation Conference (LAPC), Loughborough, 2012
51 Reed D. Experiments with spatial correlation for evaluating OTA techniques TD (09)856. COST2100, 2009. 1–4
52 Fan W, de Lisbona X C B, Sun F, et al. Emulating spatial characteristics of MIMO channels for OTA testing. IEEE Trans Antenn Propag, 2013, 61: 4306–4314
53 Boyd S, Vandenberghe L. Convex Optimization. Cambridge: Cambridge University Press, 2004
54 Llorente I C, Fan W, Pedersen G F. MIMO OTA testing in small multiprobe anechoic chamber setups. Antenn Wirel Propag Lett, 2016, 15: 1167–1170
55 Parveg D, Laitinen T, Khatun A, et al. Calibration procedure for 2-D MIMO over-the-air multi-probe test system. In: Proceedings of the 6th European Conference on Antennas and Propagation (EUCAP), Prague, 2012. 1594–1598
56 Kotterman W A T, Heuberger A, Thomä R S. On the accuracy of synthesised wave-fields in MIMO-OTA setups. In: Proceedings of the 5th European Conference on Antennas and Propagation (EUCAP), Rome, 2011. 2560–2564
57 Laitinen T A, Kyösti P, Nuutinen J-P, et al. On the number of OTA antenna elements for plane-wave synthesis in a MIMO OTA test system involving a circular antenna array. In: Proceedings of the 4th European Conference on Antennas and Propagation (EUCAP), Barcelona, 2010
58 Schirmer C, Landmann M H, Kotterman W A T, et al. 3D wave-field synthesis for testing of radio devices. In: Proceedings of the 8th European Conference on Antennas and Propagation (EuCAP), Hague, 2014. 3394–3398
59 Fan W, Kyosti P, Hentila L, et al. Rician channel modeling for multiprobe anechoic chamber setups. Antenn Wirel Propag Lett, 2014, 13: 1761–1764
60 Ji Y L, Fan W, Pedersen G F, et al. On channel emulation methods in multiprobe anechoic chamber setups for over-the-air testing. IEEE Trans Veh Technol, 2018, 67: 6740–6751
61 Giacaglia G E O. Trigonometric Interpolation. Celestial Mech, 1970, 1: 360–367
62 Fan W, Hentila L, Kyosti P, et al. Test zone size characterization with measured MIMO throughput for simulated MPAC configurations in conductive setups. IEEE Trans Veh Technol, 2017, 66: 10532–10536
63 Fan W, Kyosti P, Nielsen J Ø, et al. Wideband MIMO channel capacity analysis in multiprobe anechoic chamber setups. IEEE Trans Veh Technol, 2016, 65: 2861–2871
64 Jungnickel V, Jaeckel S, Thiele L, et al. Capacity measurements in a cooperative MIMO network. IEEE Trans Veh Technol, 2009, 58: 2392–2405
65 Laitinen T, Toivanen J, Kyösti P, et al. On a MIMO-OTA testing based on multi-probe technology. In: Proceedings of URSI International Symposium on Electromagnetic Theory, Berlin, 2010. 227–230
66 Kyösti P, Nuutinen J, Jämsä T. Simulated correlation accuracy of MIMO OTA spatial fading emulator. In: Proceedings of the 11th MCM COST-2100, Alborg, 2010
67 Imai T, Okano Y, Koshiro K, et al. Theoretical analysis of adequate number of probe antennas in spatial channel emulator for MIMO performance evaluation of mobile terminals. In: Proceedings of the 4th European Conference on Antennas and Propagation (EuCAP), Barcelona, 2010
68 Panasonic and Tokyo Institute of Technology. Procedure of the determining the dimension of a spatial fading emulator. In: Proceedings of 3GPP TSG RAN4 Meeting, Jeju, 2009
69 Laitinen T, Kyösti P, Jämsä T, et al. Generation of a field with a laplacian-distributed power azimuth spectrum scattered by a single cluster in a MIMO-OTA test system based on multiple probe antennas. In: Proceedings of Asia-Pacific Microwave Conference, Yokohama, 2010. 2127–2130
70 Khatun A, Laitinen T, Kolmonen V M, et al. Dependence of error level on the number of probes in over-the-air multiprobe test systems. Int J Antenn Propag, 2012, 2012: 1–6
71 Khatun A, Kolmonen V M, Laitinen T, et al. Clarification of uncertainties in MIMO over-the-air multi-probe test systems. In: Proceedings of the 7th European Conference on Antennas and Propagation (EuCAP), Gothenburg, 2013. 1427–1431
72 Scannavini A, FogedL J, Gross N, et al. Test zone characterization for the multiprobe anechoic chamber setup (MPAC). In: Proceedings of the 10th European Conference on Antennas and Propagation (EuCAP), Davos, 2016
73 Fan W, Kyosti P, Ji Y L, et al. Experimental evaluation of user influence on test zone size in multi-probe anechoic chamber setups. IEEE Access, 2017, 5: 18545–18556
74 Yamamoto A. Procedure of designing the structural parameters of a spatial fading emulator with a Laplacian angular power spectrum of incoming wave. In: Proceedings of COST 2100 TD(10)10016, Athens, 2010
75 Kyösti P, Hentilä L. Criteria for physical dimensions of MIMO OTA multi-probe test setup. In: Proceedings of the 6th European Conference on Antennas and Propagation (EUCAP), Prague, 2012. 2055–2059
76 Wang W M, Wang H, Gao H Q, et al. Plane wave compensation technique for multiple-input multiple-output over-the-air testing in small multi-probe anechoic chamber. IET Microwave Antenn Propag, 2019, 13: 2625–2631

77 Fan W, Pedersen G F, Kyösti P, et al. Recent advances on OTA testing for 5G antenna systems in multi-probe anechoic chamber setups. In: Proceedings of the 6th Asia-Pacific Conference on Antennas and Propagation (APCAP), Xi'an, 2017

78 Reed D, Borsato R, Rodriguez-Herrera A. Evaluation of devices with adaptive antennas using over the air techniques. In: Proceedings of the 10th European Conference on Antennas and Propagation (EUCAP), Davos, 2016

79 Fan W, Kyosti P, Rumney M, et al. Over-the-air radiated testing of millimeter-wave beam-steerable devices in a cost-effective measurement setup. IEEE Commun Mag, 2018, 56: 64–71

80 Fan W, Zhang F C, Jämsä T, et al. Reproducing standard SCME channel models for massive MIMO base station radiated testing. In: Proceedings of the 11th European Conference on Antennas and Propagation (EUCAP), Paris, 2017. 3658–3662

81 Fan W, Carton I, Kyosti P, et al. A step toward 5G in 2020: low-cost OTA performance evaluation of massive MIMO base stations. IEEE Antenn Propag Mag, 2017, 59: 38–47

82 Fan W, Zhang F C, Wang Z P. Over-the-air testing of 5G communication systems: validation of the test environment in simple-sectored multiprobe anechoic chamber setups. IEEE Antenn Propag Mag, 2021, 63: 40–50

83 Wang H, Wang W M, Wu Y, et al. Probe selection for 5G massive MIMO base station over-the-air testing. Antenn Wirel Propag Lett, 2020, 19: 1998–2002

84 Qiao Z L, Xie Y J, Wang Z P, et al. Exploring OTA testing for massive MIMO base stations in small region. In: Proceedings of the 6th Asia-Pacific Conference on Antennas and Propagation (APCAP), Xi'an, 2017

85 Li Y L, Xin L J, Zhang X. On probe weighting for massive MIMO OTA testing based on angular spectrum similarity. Antenn Wirel Propag Lett, 2019, 18: 1497–1501

86 Pei H L, Chen X M, Fan W, et al. Comparisons of channel emulation methods for state-of-the-art multi-probe anechoic chamber based millimeter-wave over-the-air testing. In: Proceedings of the 90th Vehicular Technology Conference (VTC2019-Fall), Honolulu, 2019

87 Kotterman W A T, Schirmer C, Landmann M H, et al. New challenges in over-the-air testing. In: Proceedings of the 11th European Conference on Antennas and Propagation (EUCAP), Paris, 2017. 3676–3678

88 Khatun A, Haneda K, Heino M, et al. Feasibility of multi-probe over-the-air antenna test methods for frequencies above 6 GHz. In: Proceedings of Loughborough Antennas and Propagation Conference (LAPC), Loughborough, 2015

89 Hekkala A, Kyösti P, Kyröläinen J, et al. Performance evaluation of sectored MPAC for 5G UE antenna systems. In: Proceedings of the 6th Asia-Pacific Conference on Antennas and Propagation (APCAP), Xi'an, 2017

90 Gao H Q, Wang W M, Fan W, et al. Beam probability metric for 5G OTA testing in multi-probe anechoic chamber setups. In: Proceedings of IEEE International Symposium on Antennas and Propagation and USNC-URSI Radio Science Meeting, Atlanta, 2019. 1847–1848

91 Zhang F C, Fan W, Ji Y L, et al. Performance testing of massive MIMO base station with multi-probe anechoic chamber setups. In: Proceedings of the 12th European Conference on Antennas and Propagation (EuCAP), London, 2018

92 Gao H Q, Wang W M, Fan W, et al. Beam probability metric for OTA testing of adaptive antenna systems in multi-probe anechoic chamber setups. In: Proceedings of the 13th European Conference on Antennas and Propagation (EuCAP), Krakow, 2019

93 Kyösti P, Hentilä, Kyröläinen, et al. Emulating dynamic radio channels for radiated testing of massive MIMO devices. In: Proceedings of the 12th European Conference on Antennas and Propagation (EuCAP), London, 2018

94 Pei H L, Chen X M, Zhang M, et al. Over-the-air testing of 5G millimeter-wave system with adaptive beamforming. In: Proceedings of IEEE MTT-S International Wireless Symposium (IWS), Guangzhou, 2019

95 Zhang X, Qiao S B, Peng M G, et al. Probe selection for over-the-air test in 5G base stations with massive multiple-input multiple-output. China Commun, 2019, 16: 1–12

96 Wang H, Wang C Q, Wang W M, et al. Flexible OTA probe setups for massive MIMO base station testing. In: Proceedings of Asia-Pacific Microwave Conference (APMC), Kyoto, 2018. 908–910

97 Kyosti P, Fan W, Pedersen G F, et al. On dimensions of OTA setups for massive MIMO base stations radiated testing. IEEE Access, 2016, 4: 5971–5981

98 Kyösti P, Fan W, Kyröläinen J. Assessing measurement distances for OTA testing of massive MIMO base station at 28 GHz. In: Proceedings of the 11th European Conference on Antennas and Propagation (EUCAP), Paris, 2017. 3679–3683

99 Gao H Q, Wang W M, Wu Y L, et al. A virtual over-the-air method for 5G massive MIMO base station testing with flexible virtual probes. IEEE Access, 2019, 7: 108474

100 Reyes D, Beach M, Mellios E, et al. Over-the-air test method for 5G mmWave devices with beamforming capabilities. In: Proceedings of IEEE Globecom Workshops (GC Wkshps), Abu Dhabi, 2018